Functional validation for TNNT2 variants using patient specific iPSC-derived cardiomyocyte in dilated cardiomyopathy

Chun, Kyeong-Hyeon

Department of Medicine

Graduate School

Yonsei University

Functional validation for TNNT2 variants using patient specific iPSC-derived cardiomyocyte in dilated cardiomyopathy

Advisor Kang, Seok-Min

A Dissertation Submitted
to the Department of Medicine
and the Committee on Graduate School
of Yonsei University in Partial Fulfillment of the
Requirements for the Degree of
Doctor of Philosophy in Medical Science

Chun, Kyeong-Hyeon

June 2025

Functional validation for TNNT2 variants using patient specific iPSC-derived cardiomyocyte in dilated cardiomyopathy

This certifies that the Dissertation of Chun, Kyeong-Hyeon is Approved

Committee Chair	**Kim, Sangwoo**
Committee Member	**Kang, Seok-Min**
Committee Member	**Yang, Han-Mo**
Committee Member	**Oh, Jaewon**
Committee Member	**Lee, Seung-Hyun**

Department of Medicine
Graduate School
Yonsei University
June 2025

ACKNOWLEDGEMENTS

I have come to realize that it has been over five years since I began my doctoral course, and that I now stand at the very end of this journey. Along the way, I have been fortunate to receive the support and encouragement of many people, without whom I could not have come this far. Though words may fall short of fully expressing my gratitude, I would like to take this opportunity to share my sincere appreciation with all those who have walked this path with me.

First and foremost, I would like to express my deepest gratitude to my advisor, Professor Seok-Min Kang, for his invaluable guidance throughout the entire course of my doctoral research. He has offered unwavering support and inspired me in both my academic pursuits and my journey as a cardiologist.

I am also profoundly grateful to Professor Jaewon Oh, my respected senior and the one who first led me to specialize in heart failure. As a mentor, he provided deep insight at every stage of this research—from ideation to execution—and continues to be a tremendous source of learning. Without his constant support and interest, this study would not have been possible.

My heartfelt thanks also go to Professor Seung-Hyun Lee, who took on the responsibility of this research with me and contributed to it throughout almost every phase of the study. As both a clinician and a basic scientist, his passion and dedication left a lasting impression on me. Working with him, I came to understand how challenging and noble the path of a true researcher is.

I would also like to extend my sincere appreciation to Professors Han-Mo Yang and Sangwoo Kim, who generously evaluated and encouraged this dissertation from its planning to final stages. Despite their remarkable accomplishments as researchers, they remained deeply engaged in advising me, and this work would not have come to fruition without their support.

I am especially thankful to Dr. Sun-ho Lee, who contributed greatly during the early stages of this research. Her passion and dedication, evident since her time as

a student, have been truly inspiring. I sincerely hope that she will continue to advance with the same passion and commitment in all that you do.

I also wish to thank Jung-Yoon Choi, who helped me become more comfortable in the lab during the early phases of this project. Her support laid the foundation for me to overcome my initial fears of basic research.

My deep gratitude goes as well to Dr. Hyoeun Kim and Ru-Ri Lee, with whom I spent many thoughtful hours discussing and refining this research. These moments not only deepened my academic interest but also fostered my respect and admiration for those devoted to experimental science. Our time together has strengthened my desire to pursue meaningful research alongside colleagues like them. Of course, their support has been invaluable.

Finally, I am endlessly grateful to my family. To my parents, who raised me with steadfast love and laid the foundation for me to become a good physician, this achievement is yours, and I dedicate it to you. And lastly, to my beloved wife, Mun Ju Jung, who has held my soul with love and care, all the honor belongs to you. Thank you for loving me even when I’m buried in work. Your love means more to me than I can ever say—my love and gratitude are forever yours.

I am committed to continuing my growth as a physician and researcher, and to striving forward without complacency.

Sincerely,
2025.07.
Chun, Kyeong-Hyeon

TABLE OF CONTENTS

LIST OF FIGURES

LIST OF TABLES

ABSTRACT

Functional validation for TNNT2 variants using patient specific iPSC-derived cardiomyocyte in dilated cardiomyopathy

Dilated cardiomyopathy (DCM) represents a subset of non-ischemic heart failure, characterized by enlarged and poorly contractile ventricles. Approximately 30-50% of DCM are hereditary, with variant in the TNNT2 gene linked to the condition. While TNNT2 variants are implicated in DCM, their pathogenic classification often remains uncertain due to a lack of functional validation. Patient-derived induced pluripotent stem cell (iPSC)-derived cardiomyocytes (CMs) recapitulate key aspects of cardiac contractility and electrophysiology, providing a physiologically relevant platform for in vitro modeling of cardiomyopathies. This study aimed to obtain functional validation for specific TNNT2 variants in DCM patients by utilizing human iPSC-CMs.

Among DCM patients who underwent genetic testing at a tertiary hospital between January 2017 and March 2020, several TNNT2 variants were identified, including both likely pathogenic variant and variant of uncertain significance (VUS). iPSCs were generated from a 34-year-old male patient diagnosed with DCM, carrying a missense variant in TNNT2 p.Arg205Trp (R205W), which was classified as likely pathogenic, and from a 56-year-old male patient diagnosed with DCM, carrying a missense variant TNNT2 p.Lys210Met (K210M), which was classified as VUS. Control iPSCs obtained from a stem cell bank were used for comparison. These iPSCs were differentiated into cardiomyocytes and analyzed for variant-specific alterations in electrophysiological properties and calcium handling. Electrophysiological properties using multi-electrode arrays (MEA) and spontaneous Ca^{2+} transients were analyzed for both iPSC-CMs. CRISPR-Cas9-mediated gene editing was applied to generate isogenic controls and assess the reversibility of observed phenotypes.

The generated iPSCs expressed stem cell markers and differentiated into cardiomyocytes. Compared to the control iPSC-CMs, R205W iPSC-CMs exhibited shorter sarcomere lengths, higher spontaneous beating rates, lower contractility, and slower propagation velocity, as determined by MEA analysis. In contrast, K210M iPSC-CMs exhibited no significantly different findings in MEA analysis compared to the control iPSC-CMs. Additionally, Ca^{2+} transient analysis showed lower systolic Ca^{2+} and amplitude in R205W iPSC-CMs, indicating impaired Ca^{2+} handling. Following

CRISPR-Cas9-mediated correction of R205W variant to the wild-type TNNT2 sequence, functional assays demonstrated a reversal of the previously observed phenotypic abnormalities, including improvements in electrophysiological parameters and Ca^{2+} transients.

In this study, patient-specific iPSC-CM platforms were investigated to functionally evaluate TNNT2 variants associated with DCM. The likely pathogenic variant demonstrated clear abnormalities in electrophysiology and Ca^{2+} handling, which were reversed through CRISPR-Cas9-mediated gene correction, supporting its causal role in disease. In contrast, a nearby variant classified as a VUS showed no significant functional alterations, underscoring the specificity and discriminative power of this model. These findings highlight the value of iPSC-CM-based functional assays for the clinical interpretation of sarcomeric gene variants.

Key words: cardiomyopathy, gene, variant, troponin, sarcomere, TNNT2, induced pluripotent stem cell-derived cardiomyocytes, CRISPR-Cas9

1. Introduction

Heart failure is a complex syndrome of cardiac structural and/or functional abnormalities. In 2019, there were approximately 56 million heart failure patients worldwide,[1] and by 2030, the prevalence is projected to increase by 46%,[2] and treatment costs for this disease are expected to rise by 127%. Cardiomyopathies, a subgroup of heart failure, are myocardial disorders characterized by structural and functional abnormalities of the heart. They include subtypes such as hypertrophic cardiomyopathy (HCM), dilated cardiomyopathy (DCM), and arrhythmogenic cardiomyopathy, restrictive cardiomyopathy, and unclassified cardiomyopathies.[3] DCM is characterized by ventricular enlargement and impaired contractility, particularly of the left ventricle,[4] which plays a central role in maintaining cardiac output. These structural and functional abnormalities ultimately lead to a progressive decline in systolic function. The estimated prevalence of genetic DCM among patients with DCM has been reported to range from 30% to 50%,[3][5-7] and family-based studies have reported that 15–30% of DCM patients may be familial DCM if family members undergo clinical screening.[8][9] In these familial cases, about 40% are estimated to have identifiable genetic causes.[6] Additionally, among familial DCM cases, some may be attributed to a genetic cause. Furthermore, certain genes significantly increase the risk of sudden death and life-threatening ventricular arrhythmias, highlighting the critical importance of genetic variants in DCM.[10] However, since the exact prevalence of familial DCM and the genetic background is expected to vary significantly by region and race, it is inevitable to rely on studies from major countries.[4]

DCM is a disease phenotype characterized by a weakened force-generating function of myocardium. The sarcomere, the fundamental structural and functional unit of the myocardium, plays a critical role in contractile function. The troponin complex makes up the thin filament of the

sarcomere and binds with calcium, altering the position of tropomyosin.[11] The impairment of this complex leads to structural and functional changes in the sarcomere, clinically manifesting as the DCM phenotype. A large genetic study reported that troponin complex variants occur in 6% of familial DCM cases.[12] The TNNT2 gene encodes cardiac troponin T (cTnT), a part of the troponin complex, and the variant in this gene account for approximately 3% of cases of DCM patients according to the previous reports.[13-15] However, detailed functional data about the genetic effect of TNNT2 variant in DCM is limited, and its pathogenicity is less understood compared to common genes like titin, which is the most common causative gene (12–25%) in DCM.[16] Moreover, only about 13% of TNNT2 variants in ClinVar can be clearly classified as benign or pathogenic by American Medical College of Medical Genetics and Genomics (ACMG) criteria.[13][17] This is attributed to low population allele counts, few linkage studies, and a high frequency of missense variants that are difficult to assess by *in silico* methods.[17] Nonetheless, several studies have provided valuable information of the impact of TNNT2 variants on DCM.[13][15] A recent study analyzing genetic variants in a large DCM cohort of over 1,000 patients compared to healthy controls reported that TNNT2 was one of the key genes with a significantly higher frequency of non-truncating variants in DCM patients.[18] Additionally, recent literature suggested that TNNT2 missense variants may possess high pathogenic potential,[13] while truncated TNNT2 variants are rarely reported.[19] This highlights the necessity for further research to elucidate the variants in TNNT2 gene, especially non-truncating variant. Consequently, functional validation for each variant in the TNNT2 gene remains essential, contingent on their specific location and associated clinical scenarios.

Various methods have been attempted for functional validation of such genetic variations, but certain approaches may be limited by physiological relevance or technical feasibility. For example, conventional mouse models are limited by fundamental interspecies differences in cardiac physiology and gene expression between mice and humans.[20][21] Primary adult cardiomyocytes also

pose technical challenges due to low survival rates and limited proliferative capacity,[22] poor amenability to gene editing,[23] and high demands in time and cost,[24][25] thereby restricting their use in functional studies of genetic variants. As an alternative, human induced pluripotent stem cell (iPSC)-derived cardiomyocytes (CMs), are widely used in research and preclinical safety pharmacology, advancing knowledge of human heart physiology, pathology, and pharmacology. Patient-derived iPSC from peripheral blood mononuclear cells can be differentiated into cardiomyocytes with over 90% efficacy, mimicking cardiac contractility and electrophysiology, thus providing a platform for *in vitro* modeling of cardiomyopathies.[26] Compared to primary cardiomyocyte cell lines, iPSCs provide a more suitable platform for gene evaluation and functional investigations.[27] By combining iPSC technology with CRISPR-Cas9 gene editing technology,[28] disease models can be created to better understand disease mechanisms and validate causal genes by correcting genetic variants, thereby confirming their genetic contribution.

In this study, iPSCs-derived CM model from DCM patients was used to validate the link between TNNT2 variants and DCM. Two DCM patients carrying different TNNT2 variants were recruited for this study. The clinical profiles of the patients were evaluated, and bioinformatics analysis was performed for each of the genetic variants. iPSC-CMs were generated and examined for their potential as a functional validation model for genetic DCM. Electrophysiology and calcium transient measurements were conducted to assess the impact of TNNT2 variants on cardiomyocyte function. Additionally, CRISPR-Cas9 gene editing was employed to investigate structural and functional changes in mutant iPSC-CMs.

2. Materials and Methods

2.1. Ethical statement

This research was conducted following approval from the Institutional Review Board and Ethics Committee of the Yonsei University Health System (IRB No. 4-2020-0112). Prior to participation, all patients provided written informed consent.

2.2. Patient selection for TNNT2 variants and hypothesis

The initial objective was to identify patients who had been diagnosed with DCM associated with TNNT2 variants. These patients were selected from those who underwent genetic studies for heart disease (including heart failure, arrhythmia, and cardiomyopathy) at a single tertiary hospital between January 2017 and March 2020, focusing specifically on those diagnosed with DCM. Diagnosis was based on each patient's clinical history, imaging studies of coronary artery, and echocardiography data. Patients with ventricular systolic failure (left ventricular ejection fraction ≤40%) and a dilated left ventricle were classified as having DCM. For genetic analysis, a total of 369 genes related to inherited cardiovascular disease were screened using an in-house next-generation sequencing (NGS) panel for each patient. Synonymous variants were excluded from the analysis, as they were considered less likely to result in functional alterations. In the screened DCM cohort, six TNNT2 gene variants were identified in patients with DCM. These variants are listed in **Table 1**. All these variants were missense variants. According to the ACMG criteria, two were classified as pathogenic (p.Arg92Trp, p.Arg141Gln), one as likely pathogenic (p.Arg205Trp), and three as variants of uncertain significance (VUS) (p.Lys210Met, p.Ala27Gly, and p.Gly285Arg). Among these variants, the two variants classified as pathogenic had already been well-documented

with sufficient supportive evidence,[29)30)] reducing the need for further validation. The variant classified as likely pathogenic was p.Arg205Trp, which had some prior clinical and functional experimental evidence supporting its pathogenicity. However, it had not been definitively established as a clearly pathogenic variant. Additionally, as one of the VUS variants, p.Lys210Met was near p.Arg205Trp and within the same functional domain. Although several studies had investigated in-frame deletions at amino acid of position 210,[14)31)32)] there was a lack of direct evidence for this p.Lys210Met variant. Based on this, this study was designed to investigate DCM patients carrying the TNNT2 p.Arg205Trp variant (hereafter referred to as Patient 1), classified as likely pathogenic, and the TNNT2 p.Lys210Met variant (Patient 2), classified as a VUS located nearby.

It was hypothesized that the classification of TNNT2 variants suggested by bioinformatics analysis could be functionally validated by assessing the associated phenotypic alterations using an iPSC-CM model. If required, gene editing would be employed to confirm the impact of variant on the disease phenotype.

2.3. Genetic analysis and *in silico* variant assessment

Genetic analysis of the DCM cohort was performed using an in-house NGS panel as mentioned above. Massively parallel sequencing was done on the MiSeq System (Illumina, San Diego, CA, USA). Quality control and sequence analysis was done using the BaseSpace (Illumina) and NextGENE (SoftGenetics, State College, PA, USA). Genome Reference Consortium Human Build (GRCh37, hg19) was used as reference sequence for mapping and variant calling. Databases used for analysis and variant annotation include ClinVar (https://www.ncbi.nlm.nih.gov/clinvar/) and gnomAD (https://gnomad.broadinstitute.org).[33)34)] Classification of variants followed the standards

and guidelines established by the ACMG.[17] All pathogenic and likely pathogenic variants were further confirmed by Sanger sequencing.

To assess the intolerance of the TNNT2 gene to loss-of-function (LoF) variants, the probability of LoF Intolerance (pLI) score was obtained from the gnomAD.[35] The pLI score is a gene-level metric that estimates the probability that a given gene is intolerant to heterozygous LoF variants, based on the observed versus expected number of such variants across large human cohorts. A score near 1.0 indicates strong LoF constraint, while a score near 0.0 suggests LoF tolerance. Additionally, to assess the gene-level intolerance to missense variation, the missense Z score was obtained from the gnomAD database. This score reflects the deviation between the observed and expected number of missense variants in a gene, with higher scores indicating stronger selective constraint.

To evaluate the conserved profile of each genetic variant, conservation scoring were assessed using phastCons100 score system.[36][37] PhastCons100 score reflects the degree of evolutionary conservation across 100 vertebrate species; scores near 1 indicate highly conserved and potentially functionally important regions. This high level of evolutionary conservation suggests that the position is likely to be functionally important, and alterations at this site may have a greater potential for pathogenicity. In addition, the potential protein-damaging effect of each amino acid substitution was assessed using the PolyPhen-2 score system (http://genetics.bwh.harvard.edu/pph2/).[38] PolyPhen-2 is a predictive model designed to assess the potential impact of amino acid substitutions on the structure and function of a protein. It provides a score ranging from 0 to 1, where higher scores indicate a greater likelihood of the variant being deleterious. PolyPhen-2 provides two predictive models: HumDiv, optimized for rare, high-impact variants typically associated with Mendelian diseases, and HumVar, calibrated for broader clinical use, including both rare and common variants. According to this classification, variants with scores >0.9 are classified as ‘probably damaging’ in both models. To enhance the reliability of *in silico* pathogenicity prediction,

Sorting Intolerant From Tolerant (SIFT) scores were utilized in parallel.[39] SIFT scores were used to assess evolutionary conservation and the potential functional impact of the amino acid substitution. According to the SIFT algorithm, variants with scores ≤0.05 are predicted to be deleterious. When combined with PolyPhen-2 predictions, the consistent deleterious classification supported application of supporting evidence for pathogenicity (PP3) criterion.[17]

2.4. iPSC generation and cardiomyocyte differentiation

Peripheral blood mononuclear cells (PBMCs) were obtained from the patients described above. PBMC isolation was conducted using the SepMate™ system (StemCell Technologies, Vancouver, Canada) following the manufacturer's instructions. Reprogramming into iPSCs was achieved using the Epi5™ Episomal iPSC Reprogramming Kit (Thermo Fisher Scientific, A15960), which contains five transcription factors—Oct4, Sox2, Lin28, Klf4, and L-Myc. The absence of episomal vectors in the derived iPSC lines was verified by polymerase chain reaction (PCR) at passage 20. The established iPSCs were cultured in TeSR-E8 medium (StemCell Technologies) on vitronectin-coated plates and passaged every four days using ReLeSR reagent (StemCell Technologies). For cardiac differentiation,[40] cells were plated onto Matrigel-coated six-well plates and cultured until ~90% confluency. At that point, they were treated with RPMI 1640 medium (Gibco-RBL) supplemented with B27 minus insulin (A1895601, Gibco™, USA) and 10 μM CHIR99021 (Tocris, Minneapolis, MN, USA) to activate the Wnt signaling pathway and induce mesoderm lineage specification. Three days later, the media was changed to RPMI 1640 plus B27 minus insulin with the Wnt inhibitor C59 (Selleckchem, Boston, MA, USA). After 48 hours, cells were maintained in RPMI 1640 supplemented with either B27 minus insulin or B27 (A17504044, Gibco™, USA). To enrich cardiomyocytes, metabolic selection was carried out using glucose-depleted RPMI 1640 medium

supplemented with B27, as previously described.[41)]

2.5. Immunocytochemistry

Pluripotency of iPSCs cultured on Matrigel™-coated chamber slides was assessed via immunocytochemical staining. Cells were fixed in 4% paraformaldehyde for 20 minutes at room temperature, followed by permeabilization and blocking in a PBS solution containing 3% bovine serum albumin (LPS solution, 9048–46-8) and 0.3% Triton X-100 (USB®, 9002-93-1). Primary antibodies targeting OCT4, SOX2, SSEA4, and TRA-1-60 were applied and incubated overnight at 4°C. After two PBS washes, cells were incubated at room temperature for 3 hours with Alexa® Fluor 488-conjugated chicken anti-rabbit IgG (1:500, Thermo Fisher Scientific, A21441) or Alexa® Fluor 546-conjugated goat anti-mouse IgG (1:500, Thermo Fisher Scientific, A11030) as secondary antibodies. Nuclear staining was carried out using Hoechst 33342 (Thermo Fisher Scientific, 62249). Imaging was performed using a confocal laser scanning microscope (LSM710, Zeiss), and data were analyzed using ZEN software. Detailed information regarding the antibodies, including their working dilutions used in this study, can be found in **Table 2**.

Table 1. List of TNNT2 variants identified in the DCM cohort

No.	ACMG classification	Rs number (dbSNP)	cDNA	Amino-acid	Allele frequency
1	P	rs397516456	c.274C>T	p.Arg92Trp	0.000006
2	P	rs730881101	c.422G>A	p.Arg141Gln	0.000026
3	LP	rs45586240	c.613C>T	p.Arg205Trp	0.000001
4	VUS	rs190805300	c.629A>T	p.Lys210Met	0.000011
5	VUS	rs776406819	c.80C>G	p.Ala27Gly	0.000002
6	VUS	rs147940106	c.853G>A	p.Gly285Arg	0.000001

All allele frequencies were analyzed from the gnomAD database and are reported to six decimal places for consistency.
Abbreviations: DCM, dilated cardiomyopathy; ACMG, American Medical College of Medical Genetics and Genomics; Rs, reference single nucleotide polymorphism; dbSNP, The Single Nucleotide Polymorphism Database; P, pathogenic; LP, likely pathogenic; VUS, variant of uncertain significance.

Table 2. The antibodies used for immunostaining

	Antibody	Supplier	Cat no.	Dilution
Pluripotency Markers (Immunocytochemistry)	**SSEA-4**	Thermo Fisher Scientific	46-8843-42	1:100
	OCT4	Cell Signaling Technology	9656	1:300
	SOX2	Thermo Fisher Scientific	53-9811-82	1:100
	TRA-1-60	Thermo Fisher Scientific	13-8863-82	1:100
Pluripotency Markers (Flow cytometry)	**SOX2**	Thermo Fisher Scientific	53-9811-82	0.25 μg/test
	TRA-1-60	Thermo Fisher Scientific	12-8863-82	0.5 μg/test
	SSEA-4	Thermo Fisher Scientific	46-8843-42	0.03 μg/test
	OCT3/4	Thermo Fisher Scientific	50-5841-80	0.5 μg/test
Trilineage Differentiation Markers	**NeuN**	Thermo Fisher Scientific	PA5-78639	1:100
	TuJ-1	R&D Systems	MAB1195	1:100
	Nkx2.5	Thermo Fisher Scientific	PA5-49431	1:100
	Brachyury	R&D Systems	AF2085	1:100
	SOX17	R&D Systems	AF1924	1:100
	FOXA2	Thermo Fisher Scientific	PA5-35097	1:100

Abbreviations: SSEA4, stage-specific embryonic antigen 4; OCT4, octamer-binding transcription factor 4; TRA-1-60, podocalyxin; Sox2, SRY-box transcription factor 2; Nkx2.5, NK2 homeobox 5; NeuN, Neuronal Nuclei; TuJ-1, Neuron-specific class III β-tubulin; Brachyury, T-box transcription factor T; SOX17, SRY-Box Transcription Factor 17; FOXA2, Forkhead Box A2.

2.6. Plasmid construction, gene editing, and transfection

CRISPR-Cas9 system was used to perform genome editing in the patient derived iPSC-CMs, modifying the TNNT2 variant to a wild-type sequence. The plasmid pSpCas9(BB)-2A-Puro V2.0 (px459; plasmid derived from Streptococcus pyogenes containing the endonuclease Cas9 gene) was used, a widely used plasmid for CRISPR-Cas9-mediated editing. This vector contains the Cas9 coding sequence, a gRNA scaffold, and a puromycin resistance gene, allowing for selection of successfully transfected cells.

Single-guide RNA (sgRNA) targeting the region adjacent to 613T of TNNT2 was designed using the online CRIPSR design tool. The sgRNA was selected from candidates with a high predicted gene editing score and was designed as shown in **Table 3**. The sgRNA target sites are underlined. The sgRNA sequence involved sticky end of BbsI restriction enzyme indicated in italic (Forward primer: CACC, Reverse primer: AAAC). The double-stranded oligonucleotide consisting of the forward and reverse gRNA was subcloned into the pX459 plasmid. The single-strand oligo deoxynucleotide (ssODN) was designed to correct the TNNT2 variant of Patient 1, the sequence is shown in **Table 3**. Phosphorothioate bonds were also introduced between 3 nucleotides at 5' and 3'ends of ssODN, to prevent their degradation by endogenous nucleases and thereby increasing the effective concentration of ssODN available during the DNA repair.

The constructed pX459-sgRNA plasmid and ssODN were electroporated into Patient 1 iPSCs using the Neon electroporation system with the conditions of 850 V, 30 ms, and 2 pulses. The resulting plasmid and ssODN were introduced into iPSCs derived from the patient via electroporation. One day after electroporation, the mTeSR1 medium (Stemcell Technologies, Vancouver, Canada) was replaced mTeSR1 medium with puromycin (Sigma-Aldrich, Saint Louis, MO, USA) at a final concentration of 1 μg/ml. After 24 h of selection, the selection culture medium

was changed to normal mTeSR1 medium, and the viable cells were detached and seeded in a 96-well plate at a density of 1 cell per well. After 2 months of culture, a homogenous colony was successfully obtained. The genomic DNA was extracted from each clone using QuickExtract DNA Extraction Solution (Biosearch Technologies, Hoddesdon, U.K.). Sequences adjacent to the targeting sites were amplified and analyzed to confirm accurate gene correction by Sanger sequencing.

Table 3. sgRNA and ssODN sequences for gene editing

Category	Sequence
sgRNA	F: 5'-CACCGTGGGAAGAGGCAGACTGAGT-3' R: 5'-AAACACTCAGTCTGCCTCTTCCCAC-3'
ssODN	5'-CCAGACAGAGCGGAAAAGTGGGAAGAGGCAGACTGAGCGGGAAA AGAAGAAGAAGATTCTGGCTGAGAGGAGG-3'

The underlined base ('C') represents the intended point mutation introduced via ssODN-mediated homology-directed repair, corresponding to a T-to-C substitution at codon base 613 (exon 14) of the TNNT2 gene, resulting in p.Arg205Trp amino acid change.
Abbreviations: sgRNA, single-guide ribonucleic acid; ssODN, single-strand oligo deoxynucleotide; F, forward; R, reverse.

2.7. Multi-electrode array recording and analysis

The iPSC-derived cardiomyocytes were seeded on multi-well Multi-electrode array (MEA) plates (M384-tMEA-24W; Axion BioSystems, Atlanta, Georgia, USA) and data were acquired using the Maestro Edge MEA platform (Axion BioSystems, Atlanta, Georgia, USA). A total of 50,000 cells were seeded as a 5 μL droplet in the center of each well, and an additional 500 μL of medium was carefully added after one hour. The culture medium was replaced every two days, and electrophysiological activity began to emerge as the cardiomyocytes matured. MEA-based electrophysiological analysis was conducted 7 to 10 days after re-plating the differentiated, spontaneously beating iPSC-derived cardiomyocytes, to allow stabilization of baseline electrical signals and re-establishment of a functional syncytium. Recordings were obtained using the Maestro Edge MEA platform (Axion Biosystems, Atlanta, GA, USA). Signals were filtered using a 0.1–2.0 kHz band-pass filter, with a beat detection threshold set at 300 μV. Field potential data were analyzed via the integrated software, providing metrics such as beat period (seconds), spike amplitude (μV), and field potential duration (FPD, milliseconds). Contractile performance was assessed using parameters including excitation-contraction delay and contraction amplitude. The excitation–contraction delay represents the time between the depolarization event and the peak of the contractility waveform, whereas contraction amplitude reflects impedance changes occurring as the cardiomyocytes contract and relax. Local extracellular action potentials (LEAP) were also recorded to evaluate action potential durations (APD) at 30%, 50%, and 90% repolarization (APD30, APD50, APD90, respectively). All recordings were obtained using the standard cardiac settings (Maestro AxIS software, Axion Biosystems, version 2.1.1.5) at 37°C.

2.8. Calcium transient assay

Differentiated iPSC-derived CMs were seeded in matrigel-coated 35mm glass bottom dishes (SPL, 100351). CMs were loaded with 5 μM Fluo-4 AM fluorescent calcium indicator (F14201, Thermo Fisher Scientific) for 20 min and then recorded in Tyrode's solution (T2397, Sigma-Aldrich) in the temperature range of 18–22℃. Spontaneous Ca^{2+} transients were acquired using a line-scan mode. A total of 10,000 images were acquired over a 61 s recording. For the Ca^{2+} transient recording, confocal line-scan imaging was performed on resting cells at 494 nm excitation and 506 nm emission using Zeiss LSM710 inverted confocal microscope at 20x magnification. The Ca^{2+} transients were processed using ZEN software (Carl Zeiss Microscopy GmbH, Germany) and analyzed using Microsoft Excel (Microsoft Corporation, Redmond, WA, USA).

2.9. Statistical analysis

To verify the assumption of normal distribution, the Shapiro–Wilk test was applied. A P-value of 0.05 or higher was interpreted as indicative of normally distributed data. Based on this assessment, comparisons between groups were carried out using either Student's t-test or one-way ANOVA followed by Tukey's post-hoc test for multiple comparisons. Data are presented as mean ± standard deviation (SD). All statistical analyses were performed using GraphPad Prism 8 (GraphPad Software, La Jolla, CA, USA). P-value < 0.05 indicates statistical significance. Statistical significance was set at * $P < 0.05$, ** $P < 0.01$, and *** $P < 0.001$.

3. Results

3.1. Patient information

Patient 1 was a male carrying missense variant (c.613C>T, p.Arg205Trp; R205W) in exon 14 of the TNNT2 gene. This abnormality was identified through a family screening test at the age of 34 years. The patient had a history of hypertension, diabetes but no other medical history. Before the patient was diagnosed, his one-year-old daughter had already been diagnosed with acute decompensated heart failure and DCM, requiring advanced heart failure therapy. As a result, the family underwent cardiac evaluation, leading to the identification of the patient's condition. Echocardiography for this patient revealed that his left ventricular contractile function was diminished, with a left ventricular ejection fraction of 44%, consistent with a diagnosis of DCM. As a pedigree on Genetic testing was performed on the patient's daughter, revealing the same TNNT2 variant (R205W) as found in the patient (**Figure 1A**). No other family members exhibited cardiac-related symptoms, and genetic testing was not conducted for them.

Patient 2 was also a male with missense variant (c.629A>T, p.Lys210Met; K210M) in the same exon of the TNNT2 gene. At the age of 56, the patient underwent cardiac evaluation due to symptoms of dyspnea and was subsequently diagnosed with DCM. His echocardiographic findings showed severely reduced left ventricular contractile function, with a left ventricular ejection fraction of 15%. The patient had no history of hypertension or other medical history. As shown in the pedigree (**Figure 1B**), no other family members had a history suggestive of DCM.

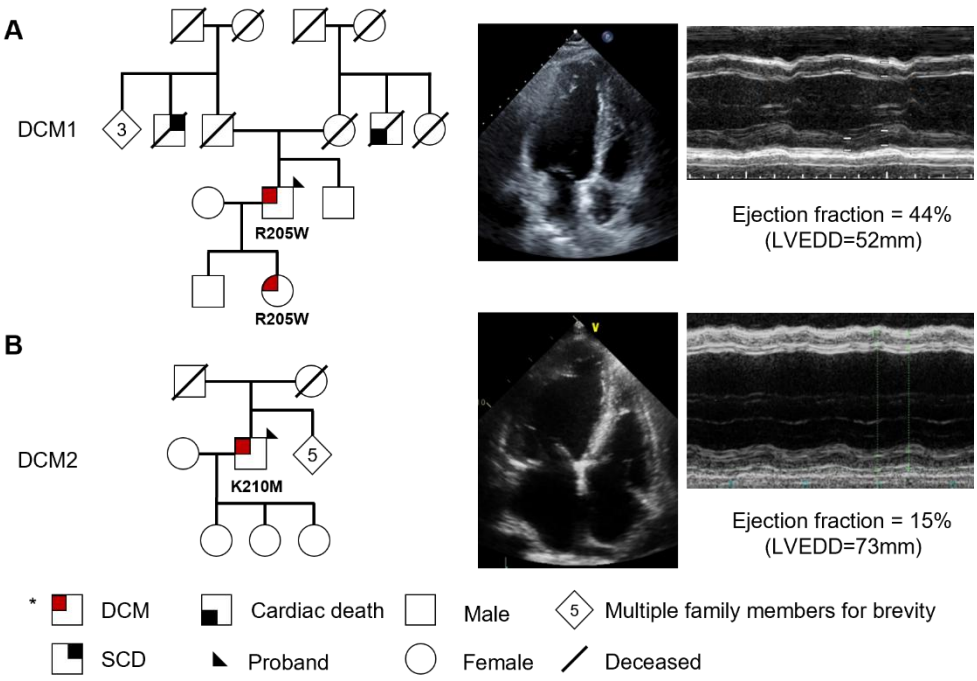

Figure 1. Overview of the pedigrees of two DCM patients and echocardiographic findings. In the pedigree diagram, squares and circles denote males and females, respectively; filled symbols indicate affected individuals, and open symbols denote unaffected individuals. (A) Patient 1 (labeled as DCM1) was a 34-year-old male identified with the TNNT2 R205W variant with family history of his one-year-old daughter, who carried the same variant. No other family members exhibited the same clinical phenotype. Patient 1 exhibited a mildly reduced LV ejection fraction (44%) with a relatively preserved LV chamber size (LVEDD=52 mm) (B) Patient 2 (labeled as DCM2) was a 56-year-old male carrying the TNNT2 K210M variant, without any family history of DCM. Patient 2 showed a markedly dilated LV chamber (LVEDD=73 mm) and severely reduced LV ejection fraction (15%).

Abbreviations: DCM, dilated cardiomyopathy; SCD, sudden cardiac death; LV, left ventricle; LVEDD, left ventricular end-diastolic dimension.

3.2. Variant information

Before discussing each variant, a summary of the TNNT2 gene is provided to contextualize the findings. According to gnomAD constraint metrics, the TNNT2 gene shows a pLI score of 0.00, indicating tolerance to heterozygous LoF variants. However, the missense Z score for TNNT2 is 2.15, suggesting a moderate constraint against missense variation, and implying that certain amino acid substitutions may be functionally significant.

The first variant, TNNT2 R205W, has previously been reported in several cases of idiopathic DCM,[14)42)43)] indicating a high probability of its association with the disease in this patient, while there have been no published data demonstrating its segregation with disease in familial DCM settings. According to the ACMG classification criteria, this variant was classified as likely pathogenic. There are several reasons why this variant was classified as likely pathogenic; the variant occurs at a known hot-spot locus for pathogenic variants, and according to the gnomAD database, the R205W variant is classified as an ultra-rare variant, with a total allele frequency of 0.000001239, suggesting a potential association with pathogenicity due to its extremely low prevalence in the general population (**Table 4**). The R205W was identified only in the European (non-Finnish) population, with 2 detected alleles out of 1,180,022 total alleles, and it was completely absent in all other ethnic groups. Regarding the conservation profile, the phastCons100 score at the R205W variant site was 0.997, indicating a high level of evolutionary conservation across 100 vertebrate species (**Table 5**). Also, the R205W variant yielded a PolyPhen-2 score of 1.000 and a SIFT score of 0.001, both indicating a strong likelihood of deleterious functional impact, which meets supporting-level pathogenic criteria according to ACMG guidelines (**Table 5**).

The classification of the R205W was supported in part by evidence from an alternative variant at the same residue, p.Arg205Leu (R205L), which has been previously demonstrated to cause

functional alterations and to segregate clearly with disease in affected families.[12] Additionally, the same variant of this study R205W in idiopathic DCM has been also evaluated by recombinant human protein method, which showed that decreased Ca^{2+} sensitivity, although it showed no alteration in force generation.[14] Taking all these factors into consideration, the p.Arg205Trp variant was classified as likely pathogenic and does not meet the criteria for a definitive pathogenic classification, as the available functional data did not provide definitive evidence of altered protein function and co-segregation data from affected families were insufficient to establish a strong causal relationship.

The second variant, K210M, has been reported with a total allele frequency of 0.00001053 in the gnomAD database (**Table 6**). It is also classified as an ultra-rare variant across multiple populations in the database, however, K210M exhibits a relatively higher allele frequency compared to the R205W. The relative difference in allele frequency between R205W and K210M raises important questions regarding their respective pathogenic potential. According to the conservation profile, the phastCons100 score at the variant site was 1.0, indicating complete evolutionary conservation across 100 vertebrate species (**Table 5**). Also, the K210M variant was predicted to be probably damaging by PolyPhen-2 (score: 0.989) and deleterious by SIFT (score: 0.017), indicating potential functional impact which meets supporting-level pathogenic criteria (**Table 5**).

There is currently no functional validation data available for the K210M variant in the context of cardiomyopathy. However, alternative variant at the same residue, K210del, has been previously demonstrated to show functional alteration and to segregate in affected families.[12] Nevertheless, the fact that K210del has been reported as a pathogenic variant does not constitute evidence for the pathogenicity of the K210M. Consequently, based on ACMG criteria, the K210M was classified as VUS.

Table 4. Analysis of the TNNT2 p.Arg205Trp variant based on gnomAD database

Genetic Ancestry Group	Allele Count	Allele Number	Number of Homozygotes	Allele Frequency
European (non-Finnish)	2	1,180,022	0	0.000002
African/African American	0	75,020	0	0
Admixed American	0	60,016	0	0
Ashkenazi Jewish	0	29,606	0	0
East Asian	0	44,872	0	0
European (Finnish)	0	64,020	0	0
Middle Eastern	0	6,062	0	0
Amish	0	908	0	0
South Asian	0	91,084	0	0
Total	2	1,614,116	0	0.000001

TNNT2 p.Arg205Trp variant was identified only in the European (non-Finnish) population, with 2 detected alleles out of 1,180,022 total alleles (actual allele frequency: 0.000001695). The variant was completely absent in all other ethnic groups, including African, East Asian, South Asian, Finnish European, Middle Eastern, Amish, and Ashkenazi Jewish populations, as analyzed from the gnomAD database. The variant was only found in heterozygous form, with no reported homozygous individuals across all populations. This suggests that the variant is extremely rare and may be associated with disease. All allele frequencies are reported to six decimal places for consistency.

Table 5. Conservation score and protein-damaging score of each TNNT2 variant

TNNT2 Variant	Conservation score	PolyPhen-2 score		SIFT
	PhastCons100	HumVar	HumDiv	
p.Arg205Trp (R205W)	0.997	0.999	1.0	0.001
p.Lys210Met (K210M)	1.0	0.979	0.989	0.017

PhastCons100 scores indicate strong evolutionary conservation across 100 vertebrate species: 1.0 for K210M and 0.997 for R205W, suggesting both variants occur at highly conserved and potentially functionally important sites. Additionally, PolyPhen-2 provides two different predictive models: HumVar and HumDiv. Both HumDiv and HumVar scores were >0.9, suggesting that the variant is probably damaging. In this study, both variants yielded scores exceeding 0.9, supporting the prediction that these amino acid substitutions are likely to be functionally disruptive. Also, both the R205W and K210M variants were predicted to be deleterious based on SIFT scores (<0.05), indicating a high likelihood of functional disruption.

Abbreviations: SIFT, Sorting Intolerant From Tolerant.

Table 6. Analysis of the TNNT2 p.Lys210Met variant based on gnomAD Database

Genetic Ancestry Group	Allele Count	Allele Number	Number of Homozygotes	Allele Frequency
Admixed American	5	60,028	0	0.000083
East Asian	3	44,866	0	0.000067
South Asian	3	91,080	0	0.000033
European (Finnish)	1	64,032	0	0.000016
European (non-Finnish)	5	11,79,876	0	0.000004
African/African American	0	75,048	0	0
Ashkenazi Jewish	0	29,606	0	0
Middle Eastern	0	6,060	0	0
Total	17	1,614,016	0	0.000011

TNNT2 p.Lys210Met variant was identified at low frequencies across multiple populations in the gnomAD database. Specifically, it was found in Admixed American (5 alleles, actual allele frequency: 0.00008329), East Asian (3 alleles, actual allele frequency: 0.00006687), South Asian (3 alleles, actual allele frequency: 0.00003294), Finnish European (1 allele, actual allele frequency: 0.00001562), and non-Finnish European (5 alleles, actual allele frequency: 0.000004238) populations. However, it was completely absent in African/African American, Ashkenazi Jewish, and Middle Eastern populations, indicating some level of population specificity. Despite being identified in multiple ancestry groups, no homozygous cases were reported, suggesting that this variant exists exclusively in a heterozygous state. All allele frequencies are reported to six decimal places for consistency.

3.3. Cellular characteristics of the patient derived iPSC-CMs

To determine whether there is difference of cellular characteristics and functional features between the TNNT2 variant carried by DCM patients and normal cardiomyocytes with wild-type TNNT2, the cardiomyocytes were differentiated from the patient-derived iPSCs and healthy donor-derived iPSCs, respectively.

First, iPSCs were generated from Patient 1. As **Figure 2** showed, the generated iPSC line exhibited a typical human embryonic stem cell-like morphology and demonstrated robust expression of pluripotency markers, including OCT4, SOX2, SSEA-4, and TRA-1-60, as confirmed by immunocytochemistry and flow cytometry (**Figure 2A, D, and E**).[44] Also, absence of mycoplasma contamination was confirmed (**Figure 2B**). The patient harbored a heterozygous missense TNNT2 variant, p.Arg205Trp (c.613C>T; R205W) (**Figure 2C**). To validate the functional alteration, healthy donor-derived iPSCs from CMC-iPSC-011 line (hereafter, control iPSCs), which were banked at the Korea National Stem Cell Bank in 2017, were used.[44][45] Before the differentiation, sanger sequencing confirmed that the control iPSCs had wild-type TNNT2 gene containing Arg in residue 205 in exon 14 of TNNT2 gene.

After the differentiation, representative immunofluorescent images of the control iPSC-CMs and R205W iPSC-CMs showed that the iPSC-CMs were stained positively for cardiac troponin-T (cTnT) (**Figure 3A**, left panel). When TNNT2 expression was quantitatively compared using relative immunofluorescence intensity, no statistically significant difference was observed between the control and R205W iPSC-CMs (**Figure 3A**, right panel). In addition, representative immunofluorescent images of sarcomere proteins, titin (green) and α-actinin (red) for each cell line were obtained (**Figure 3B**). To investigate whether variations in sarcomere content could account for differences in cardiomyocyte function, sarcomere length was analyzed, as it has been

demonstrated to be proportional to sarcomere content.[46] When analyze the peak-to-peak of the fluorescence intensity to compare the sarcomere length of these cell lines, the sarcomere length was significantly lower in the R205W than in the control iPSC-CMs (1.654 vs. 1.814 μm, p=0.0079) (**Figure 3C,D**). These results suggest that the CMs differentiated from R205W variant in TNNT2 affect sarcomere content. These observed alterations in cell structure were presumed to be associated with changes in cardiomyocyte function, thereby leading to further functional investigation.

Second, iPSCs from Patient 2 with K210M variant were also generated as introduced above. Before the differentiation, sanger sequencing confirmed that the patient-derived iPSCs had p.Lys210Met (c.629A>T; K210M) variant in one allele of this region (**Figure 4A**). The cells exhibited a typical iPSC-like colony morphology and high alkaline phosphatase activity, which were captured using fluorescence microscopy (**Figure 4B**, left panel). Immunostaining images, PCR and flow cytometry demonstrated that the K210M iPSC lines expressed pluripotency markers (**Figure 4B**, right panel). After the differentiation, immunofluorescent images of the K210M iPSC-CMs were also obtained for the cardiac troponin-T expression (**Figure 3A**). When the expression of troponin-T was quantitatively compared, no statistically significant difference was observed between the control and K210M iPSC-CMs (**Figure 3A**, right panel). Also, in iPSC-CMs carrying the K210M variant, the expression patterns of titin and α-actinin appeared comparable to those of the control in representative immunofluorescence images (**Figure 3B**). Furthermore, quantitative measurement of sarcomere length revealed no statistically significant difference between the two groups (1.831 vs. 1.814 μm, p=0.9256).

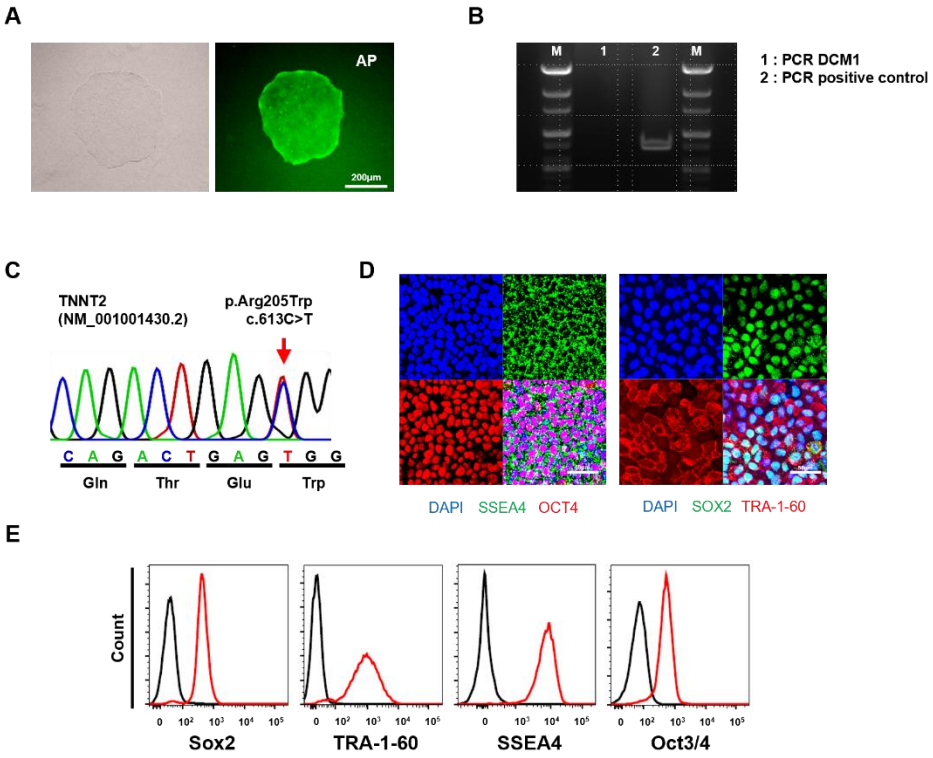

Figure 2. Characterization of iPSCs from DCM patient carrying TNNT2 R205W variant. (A) The expression of the representative pluripotency marker alkaline phosphatase was detected (scale bar, 200 μm). (B) The absence of mycoplasma contamination was confirmed using PCR and agarose gel electrophoresis. (C) Sanger sequencing showed the heterozygous c.613 C to T variant in exon 14 of the TNNT2 gene. (D) Immunocytochemistry showed the expression of pluripotency markers SSEA4, OCT4, SOX-2, and TRA-1-60 (scale bar, 50 μm). (E) Flow cytometry analysis showed the expression of Sox-2, TRA-1-60, SSEA4, and OCT3/4. Black lines were used as isotype controls.

Abbreviations: iPSC, induced pluripotent stem cell; DCM, dilated cardiomyopathy; PCR, polymerase chain reaction; SSEA4, stage-specific embryonic antigen 4; OCT4, octamer-binding transcription factor 4; Sox2, SRY-box transcription factor 2; TRA-1-60, podocalyxin.

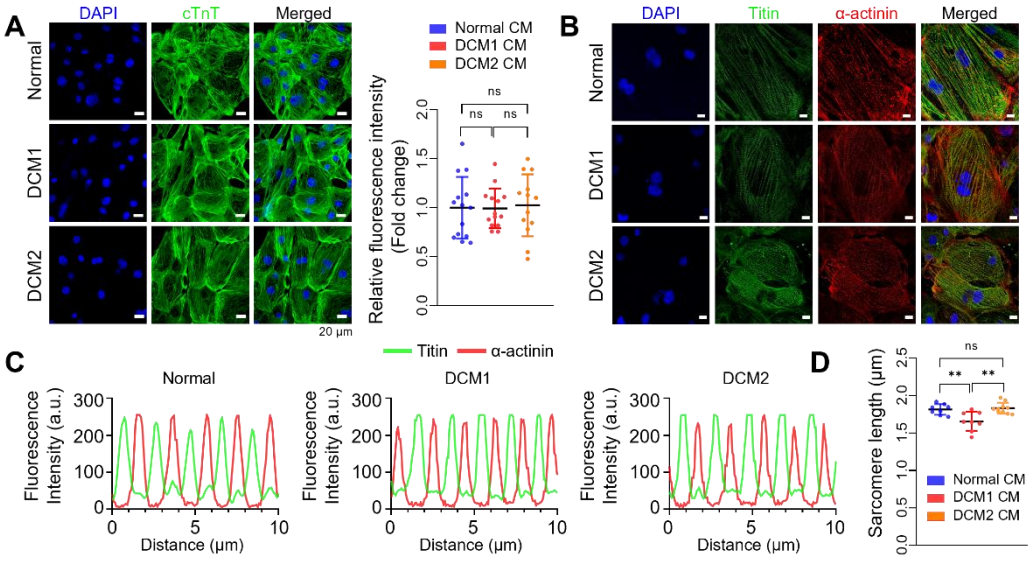

Figure 3. Characterization of iPSC-CMs from DCM patient carrying TNNT2 R205W and K210M variants. (A) Representative immunocytochemistry images of the control, R205W (labeled as DCM1), and K210M (labeled as DCM2) iPSC-CMs. The expression of cardiac specific marker, cardiac troponin T (labeled as cTnT), in each iPSC-CMs were presented. Regarding the relative fluorescence intensity, no marked difference in troponin T expression was observed between the control, DCM1, and DCM2 iPSC-CMs. (B) Representative immunocytochemistry images of sarcomere proteins, titin (green) and α-actinin (red). Also, no marked difference in titin and α-actinin expression was observed between the iPSC-CMs. (C) However, fluorescence intensity of titin and α-actinin was measured along a defined linear distance, and the spacing between peak-to-peak signals was calculated. (D) This revealed that the sarcomere length was shorter in DCM1 iPSC-CMs compared to the control and K210M iPSC-CMs, suggesting a sarcomere structural alteration only in DCM1 iPSC-CMs. ** $P < 0.01$ (Student's *t*-test).

Abbreviations: iPSC, induced pluripotent stem cell; CM, cardiomyocytes; DCM, dilated cardiomyopathy; ns, no significance.

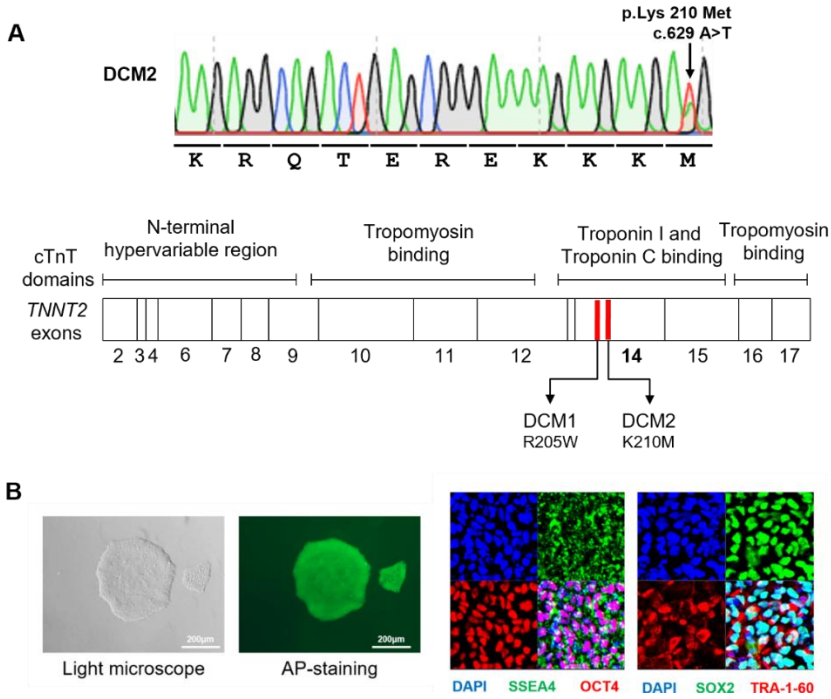

Figure 4. Characteristics of iPSCs from the patient carrying TNNT2 K210M variant. (A) Sanger sequencing showed the heterozygous c.629 A to T variant in exon 14 of the TNNT2 gene (labeled as DCM2). The TNNT2 domain schematic shows that the K210M variant lies within exon 14 and is positioned near the R205W variant, within the same functional domain. (B) The expression of the representative pluripotency marker alkaline phosphatase was detected (left, scale bar, 200 μm). Immunocytochemistry showed the expression of pluripotency markers SSEA4, OCT4, SOX-2, and TRA-1-60 (right, scale bar, 50 μm).

Abbreviations: iPSC, induced pluripotent stem cell; CM, cardiomyocyte; DCM, dilated cardiomyopathy; SSEA4, stage-specific embryonic antigen 4; OCT4, octamer-binding transcription factor 4; Sox2, SRY-box transcription factor 2; TRA-1-60, podocalyxin.

3.4. Functional characteristics of the iPSC-CMs

Cardiomyocyte is a muscle cell responsible for contraction of the heart and is characterized by electrical activation. To determine whether there is functional alteration according to the TNNT2 variant, the MEA-based non-invasive electrophysiology function was investigated. MEA can measure the electrical signals generated by cardiomyocytes in real-time to determine the beat amplitude, beat interval, conduction velocity, and can directly obtain abnormal signals such as early after depolarization (EAD) as a marker of arrhythmia. First, field potential (FP) traces data were recorded with the MEA exhibiting spontaneous beating trace for cells on the plate (**Figure 5A**, left panel) for the control and R205W iPSC-CMs. Compared to the control iPSC-CMs, R205W iPSC-CMs had a significantly lower mean of beat period than the control iPSC-CMs (1.036 vs. 1.317 sec, $p<0.001$) (**Figure 5A**, right panel), indicating the beating rate is faster in R205W iPSC-CMs than the control iPSC-CMs. Spike amplitude, which reflects voltage changes in cell membranes, was not statistically different between the two cell lines (6.05 vs. 6.18 mV, $p=0.800$). Conduction velocity was measured by MEA. The conduction plot indicated that R205W iPSC-CMs had slower conduction velocity than the control iPSC-CMs (0.038 vs. 0.065 mm/ms, $p<0.001$) (**Figure 5B**). This result suggests abnormal functioning of the cardiomyocyte due to disrupted transmission of the electrical signal or calcium ions in R205W iPSC-CMs.

Contractility was measured by MEA, which is based on the fact that when a cell attached to an electrode contracts and relaxes, the electrical signal varies depending on how the cell's surface area contacts the electrode. The beat amplitude is measured by the change in impedance while the cells are contracting and reflects the strength of the contraction force of the cells. Additionally, excitation-contraction (E-C) delay refers to the time it takes for the cardiomyocytes to contract after an electrical signal is generated. Results showed that R205W iPSC-CMs had decreased beat amplitude

(1.33 vs. 2.81%, p<0.001) and increased E-C delay (315.3 vs. 271.0 ms, p=0.002) compared to the control iPSC-CMs (**Figure 5C**). This shows that the contractile force is reduced in R205W iPSC-CMs, and the time from electrical signal to contraction is delayed.

To measure the action potential of each contraction, the LEAP assay was utilized by MEA. LEAP is efficacious for quantifying the action potential morphology of iPSC-CM in addition to FP studies.[47] Action potential duration (APD) was measured from beat start to 30%, 50%, and 90% voltage repolarization (APD30, APD50, APD90). It was observed that R205W iPSC-CMs exhibited decreased APD30, APD50, and APD90 metrics compared to the control iPSC-CMs (**Figure 5D**). These results suggest potential alterations in ion channel functions, such as decreased calcium current, which may impair excitation-contraction coupling and affect cardiac contractility.

Second, MEA analysis was also conducted to evaluate the electrophysiological characteristics of the K210M variant compared to the control iPSC-CMs (**Figure 6**). To enable this comparison, cardiomyocyte differentiation was simultaneously performed again with the control iPSCs, as in the previous experiments. At baseline FP tracing, the beating rate of the K210M iPSC-CMs was slightly faster compared to the control iPSC-CMs; the mean of beat period was significantly lower in the K210M iPSC-CMs (1.013 vs. 1.088 sec, p=0.0496) (**Figure 6A**). However, the difference was not as pronounced as that observed in R205W iPSC-CMs. Spike amplitude was not statistically different between the two cell lines (2.234 vs. 2.065 mV, p=0.323). Additionally, conduction velocity was measured, and it was not significantly different between the K210M iPSC-CMs and the control iPSC-CMs (0.059 vs. 0.06 mm/ms, p=0.853) (**Figure 6B**). This result suggests that the K210M iPSC-CMs did not show significant abnormal electrophysiologic properties except baseline beating rate.

Given that R205W iPSC-CMs displayed more significant electrophysiological differences from the control iPSC-CMs than those carrying the K210M variant, further functional evaluation of Ca^{2+}

handling dynamics was performed in the R205W iPSC-CMs. For this assessment, iPSC-CMs were replated onto Matrigel-coated glass cover slips, and their intracellular Ca^{2+} transients were measured using Fluo-4, AM (**Figure 7A**). Trace images depicted the change in fluorescence intensity (F) relative to baseline fluorescence intensity (F_0) (**Figure 7A**, lower panel). The systolic Ca^{2+} signal, which reflects Ca^{2+} influx into the cytoplasm, appeared faster and lower in amplitude in the mutant cells compared to the control iPSC-CMs. This indicates a shorter Ca^{2+} transient cycle and reduced systolic calcium levels in the diseased iPSC-CMs. Notably, quantified data revealed that R205W iPSC-CMs had significantly lower systolic calcium (F/F_0) (2.95 vs. 9.55, $p<0.001$) and calcium amplitude (F/F_0) (1.99 vs. 8.93, $p<0.001$) compared to the control iPSC-CMs. Additionally, the time to baseline (50%) (0.422 vs. 0.599 sec, $p=0.001$) and relaxation constant Tau (sec) of calcium transient (0.318 vs. 0.457 sec, $p=0.001$) were significantly shorter in R205W iPSC-CMs, indicating a faster decay (**Figure 7B**). These findings suggest that the R205W variant in TNNT2 disrupts intracellular Ca^{2+} handling dynamics, leading to reduced systolic calcium levels and an abnormally accelerated calcium decay in cardiomyocytes.

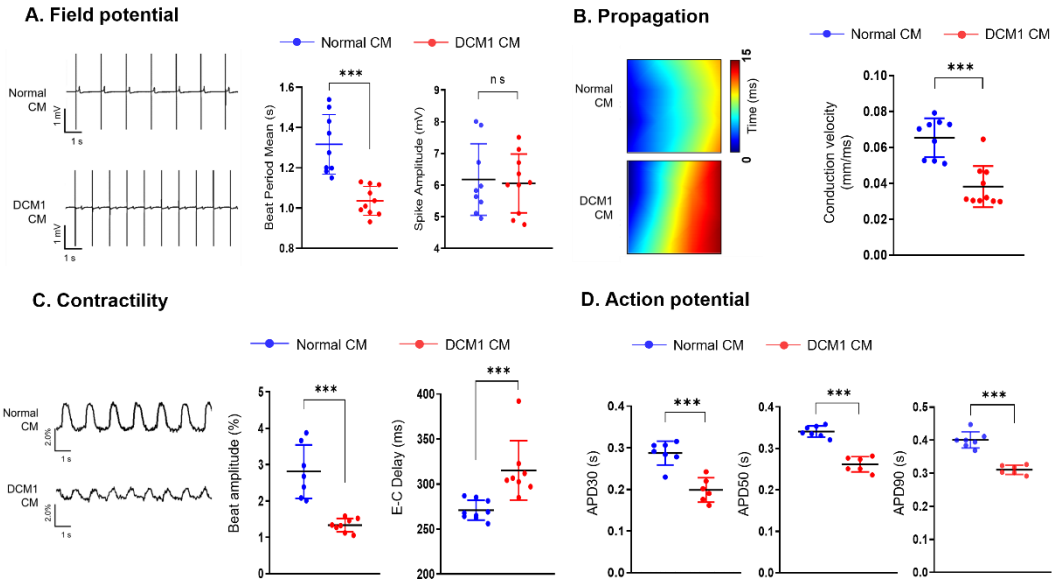

Figure 5. MEA was performed to confirm the electrophysiology in R205W iPSC-CMs. (A) Field potentials were measured by MEA. The mean of beat period was significantly lower in R205W iPSC-CMs (labeled as DCM1), while there was no difference in spike amplitude. (B) Conduction plot (left panel) showing propagation delay of cardiomyocytes, the blue region represents the origin of the beat (start electrode). The scale bar provided in the image illustrates the propagation delay time, with different colors representing varying degrees of delay. R205W iPSC-CMs had slower conduction velocity than the control iPSC-CMs. (C) Contractility was measured by change in impedance. R205W iPSC-CMs had decreased beat amplitude and increased E-C delay compared to the control iPSC-CMs. (D) The LEAP assay by MEA was obtained to monitor action potential. R205W iPSC-CMs had shorter APD30, APD50, and APD90 metrics compared to the control iPSC-CMs. *** $P < 0.001$ (Student's *t*-test).

Abbreviations: MEA, multi-electrode array; iPSC, induced pluripotent stem cell; CM, cardiomyocyte; E-C, excitation-contraction; LEAP, local extracellular action potential; ns, no significance.

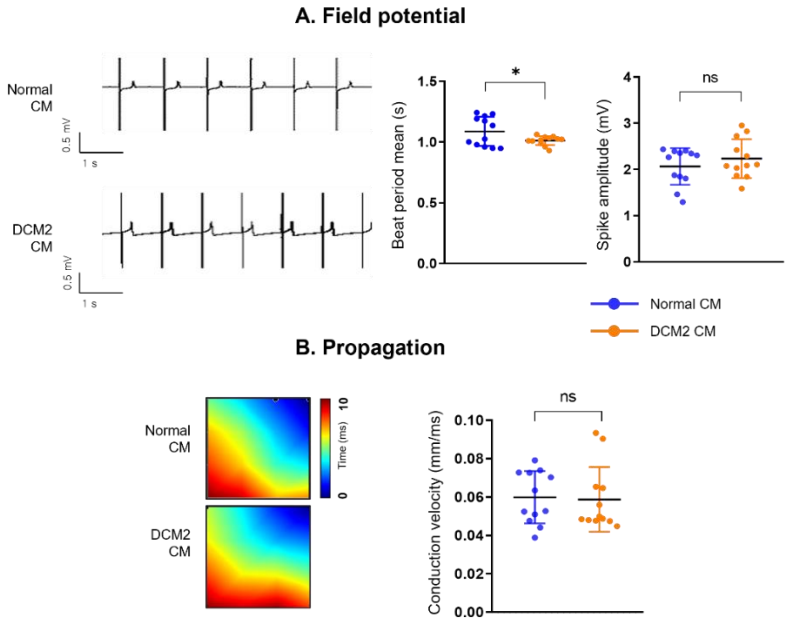

Figure 6. MEA was performed to confirm the electrophysiology in K210M iPSC-CMs. (A) Field potentials were measured by MEA. The mean of beat period was lower in K210M iPSC-CMs (labeled as DCM2), and there was no difference in spike amplitude. (B) Conduction velocity was measured. Conduction plots, which visualize propagation delay, revealed no notable differences between the two iPSC-CMs based on the scale bar and color mapping. Quantitative analysis demonstrated no significant difference in conduction velocity between the K210M and control iPSC-CMs. * $P < 0.05$ (Student's *t*-test).

Abbreviations: MEA, multi-electrode array; iPSC, induced pluripotent stem cell; CM, cardiomyocyte; ns, no significance.

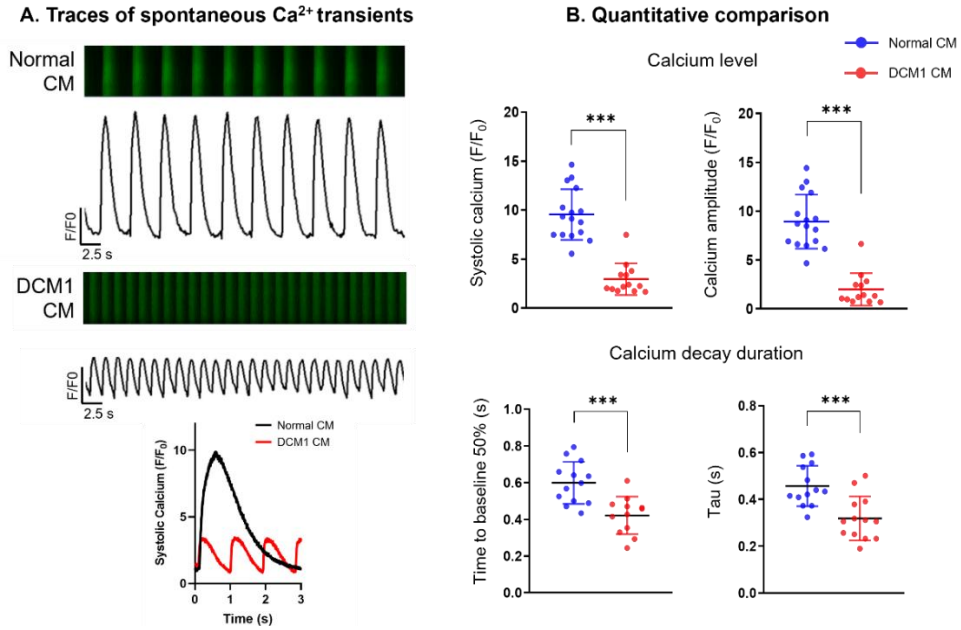

Figure 7. Calcium transient assay was performed in R205W iPSC-CMs. (A) Representative traces of spontaneous Ca^{2+} transients measured in the control and R205W iPSC-CMs (labeled as DCM1). Trace images show a change in fluorescence intensity (F) in relationship to resting fluorescence intensity (F_0). (B) R205W iPSC-CMs had significantly lower systolic calcium and calcium amplitude than the control iPSC-CMs (upper). In addition, the time to baseline (50%) and relaxation constant Tau (sec) of calcium transient were significantly shorter in R205W iPSC-CMs compared to the control iPSC-CMs (lower). *** $P < 0.001$ (Student's *t*-test).

Abbreviations: iPSC, induced pluripotent stem cell; DCM, dilated cardiomyopathy; CM, cardiomyocytes.

3.5. Cellular and ultrastructural characteristics in R205W iPSC-CMs and their rescue by gene correction

Given that R205W iPSC-CMs exhibited distinct functional alterations relative to the control iPSC-CMs in both MEA and calcium transient assays, the variant was corrected to wild-type via gene editing to assess whether the functional phenotype could be reversed. To establish the relevant isogenic lines, the CRISPR-Cas9 gene editing technique was utilized. **Figure 8** provides a schematic overview of the gene editing process. This patient exhibited a heterozygous genotype where the 613th C in exon 14 of the TNNT2 gene was substituted with a T, and the 205th amino acid, Arg, was converted to Trp (**Figure 8A**). To revert the T back to C, sgRNAs and ssODNs were constructed, and were cloned into the px459 vector (**Figure 8B, C**). The resultant corrected ($R205W^{Corr}$) iPSC revealed that the causative TNNT2 R205W variant had been rectified, demonstrating the replacement of Trp by Arg.

$R205W^{Corr}$ iPSCs were differentiated into cardiomyocytes using the same protocol applied to the unedited cells as described above. The $R205W^{Corr}$ iPSCs displayed pluripotency markers (DNMT3B, CABRB3, TDGF1) comparable to those of the control iPSC (**Figure 9**). Immunocytochemistry analysis confirmed high expression levels of pluripotency markers SSEA4, OCT4, SOX-2, and TRA-1-60.

After the differentiation, representative immunofluorescent images of R205W and $R205W^{Corr}$ iPSC-CMs showed the stained sarcomeric proteins cardiac troponin-T (**Figure 10A**). Additionally, immunofluorescent images of sarcomere proteins, titin (green) and α-actinin (red) for each cell line were obtained (**Figure 10B**). A comparison of the peak-to-peak fluorescence intensity from these cell lines indicated a significant increase in sarcomere length in $R205W^{Corr}$ iPSC-CMs compared to R205W iPSC-CMs (1.870 vs. 1.601 μm, $p<0.001$) (**Figure 10C, D**). The observed increase in

sarcomere length following correction of the R205W variant suggests that this TNNT2 mutation plays a critical role in the pathogenesis of DCM, thereby warranting further investigation into its functional consequences.

Transmission electron microscopy (TEM) was used to assess sarcomeric organization in iPSC-CMs. The control iPSC-CMs exhibited regularly spaced Z-disks and well-aligned sarcomeric structures (**Figure 11A**). In contrast, the R205W iPSC-CMs demonstrated marked ultrastructural disarray, including disorganized Z-disks and disrupted sarcomere alignment (**Figure 11B**). Following CRISPR-Cas9-mediated correction of the R205W variant, the ultrastructural phenotype was substantially restored. Corrected iPSC-CMs showed near-normal Z-line organization and sarcomeric architecture comparable to that of wild-type cells (**Figure 11C**). These findings provide direct visual evidence that the R205W variant causes structural disorganization of the sarcomere, which can be reversed through precise genetic correction.

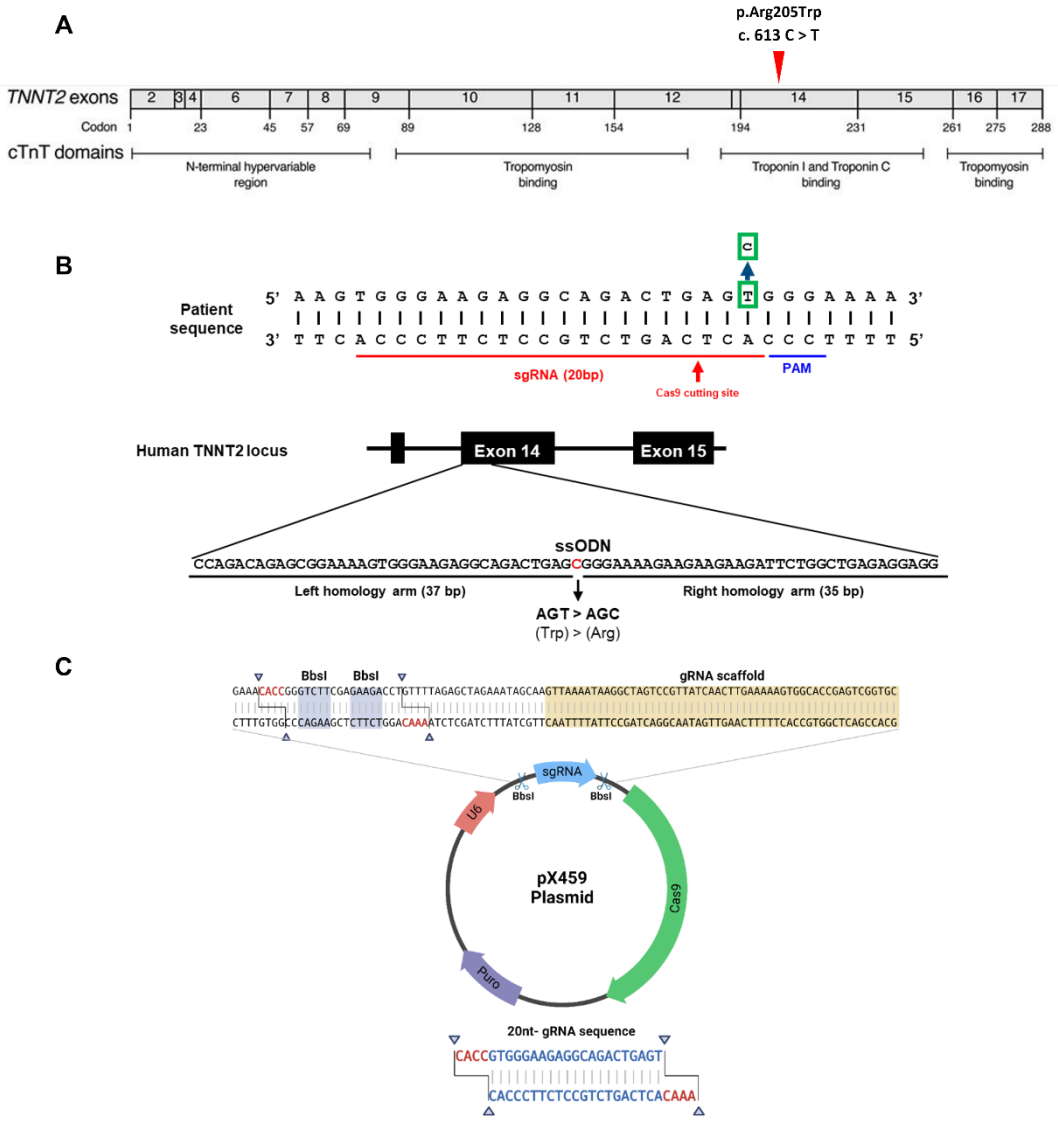

Figure 8. Schematic overview of TNNT2 gene structure, CRISPR-Cas9 sgRNA targeting, editing site, and px459 plasmid design. A schematic representation of the TNNT2 gene is shown, highlighting the location of exon 14, which contains the R205 codon targeted for editing. (A) Patient 1 carried a C-to-T point mutation at nucleotide position 613 in exon 14 of the TNNT2 gene, and gene editing was performed to revert this mutation back to the wild-type sequence (T to

C). (B) The CRISPR-Cas9 system consists of two key components: the Cas9 protein, which introduces double-strand breaks in DNA, and the sgRNA, which directs Cas9 to the target sequence. Once the sgRNA-Cas9 complex is guided to the target locus, the Cas9 protein recognizes the PAM sequence and induces site-specific DNA cleavage. Following cleavage, endogenous repair mechanisms are activated, commonly resulting in 2–3 bp insertions or deletions. For this, an sgRNA was designed for targeting the mutant locus and a ssODN containing the wild-type sequence to serve as the donor template. The sgRNA sequence designed to direct Cas9-mediated cleavage near the R205 site is displayed, along with the ssODN used for homology-directed repair. The editing strategy involves a T-to-C substitution at codon 205 to generate the R205W variant. (C) The structure of the px459 plasmid used for delivering Cas9 and sgRNA into iPSCs is also illustrated. The sgRNA was cloned into the px459 vector, a widely used plasmid for CRISPR-Cas9-mediated editing. This vector contains the Cas9 coding sequence, a gRNA scaffold, and a puromycin resistance gene, allowing for selection of successfully transfected cells.

Abbreviations: ssODN, single-stranded oligonucleotide; sgRNA, single-guide ribonucleic-acid; CRISPR-Cas9, Clustered Regularly Interspaced Short Palindromic Repeats-CRISPR-associated protein 9; PAM, protospacer-adjacent motif.

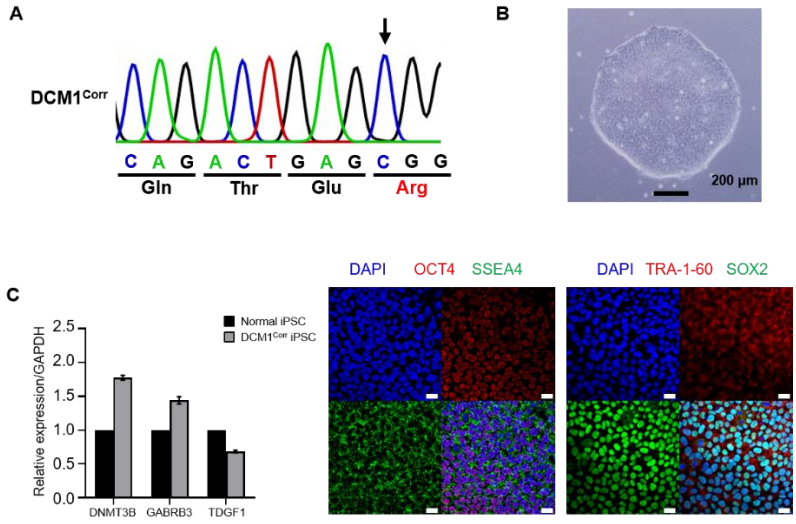

Figure 9. Characteristics of TNNT2 R205W corrected iPSCs. (A) Sanger sequencing showed that the R205W was corrected to wild type (the 613th T in R205W was exchanged to a C, Trp to Arg at the 205th amino acid). (B) Bright field image of R205W corrected (labeled as DCM1^{Corr}) iPSCs. (C) Endogenous transcript levels of pluripotency markers, DNMT3B, GABRB3, and TDGF1 were similar to the control (labeled as Normal) iPSCs, confirmed by qRT-PCR (left). Immunocytochemistry images showed high expression of the pluripotency markers, SSEA4, OCT4, SOX-2, and TRA-1-60 for the corrected R205W iPSCs (right, scale bar, 50 μm).

Abbreviations: iPSC, induced pluripotent stem cell; DNMT3B, DNA (cytosine-5)-methyltransferase 3 beta; GABRB3, gamma-aminobutyric acid type A receptor beta 3 subunit; TDGF1, teratocarcinoma-derived growth factor 1; qRT-PCR, quantitative reverse transcription polymerase chain reaction; SSEA4, stage-specific embryonic antigen 4; OCT4, octamer-binding transcription factor 4; TRA-1-60, podocalyxin; Sox2, SRY-box transcription factor 2

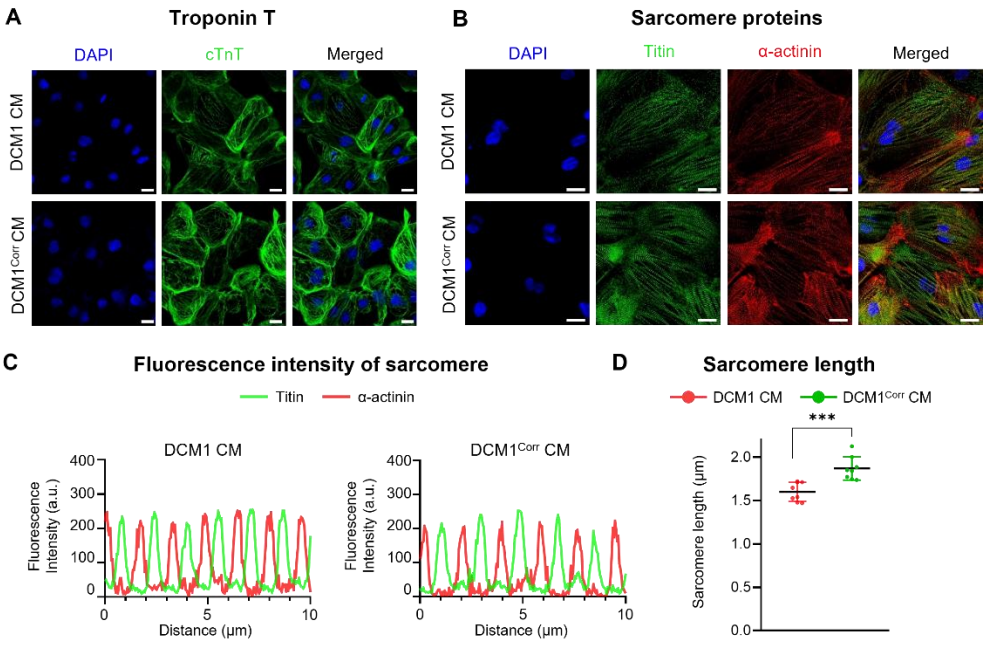

Figure 10. Characteristics of TNNT2 R205W corrected iPSC-CMs. (A) R205W iPSCs (labeled as DCM1) and R205W^{Corr} iPSCs (labeled as DCM1^{Corr}) were differentiated to CMs and there was no difference in the expression of cTnT using immunocytochemistry. (B) Immunocytochemistry images of titin and α-actinin. In both R205W and R205W^{Corr} iPSC-CMs, the sarcomere structure was well-formed. (C, D) Quantification analysis from fluorescence intensity of titin and α-actinin showed that the sarcomere length was significantly increased in the R205W^{Corr} iPSC-CMs compared to R205W iPSC-CMs. *** $P < 0.001$ (Student's *t*-test).

Abbreviations: iPSC, induced pluripotent stem cell; CM, cardiomyocytes; cTnT, cardiac troponin T.

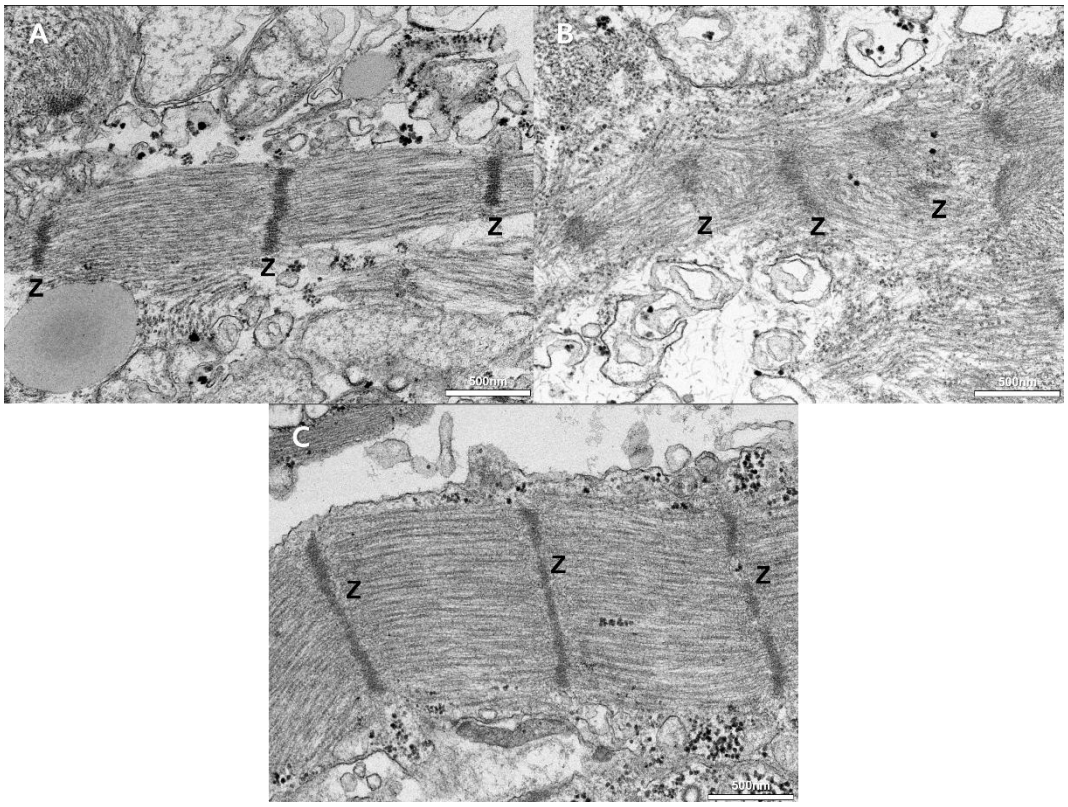

Figure 11. TEM images of cardiomyocytes derived from iPSCs. These images represent TEM images of sarcomere structures in the control, R205W, and gene-corrected R205W iPSC-CMs, respectively. (A) The control iPSC-CMs show well-organized Z-disks and intact sarcomeric alignment. (B) R205W iPSC-CMs exhibit markedly disorganized Z-disks and disrupted sarcomeric architecture. (C) Following CRISPR-mediated gene correction, $R205W^{Corr}$ iPSC-CMs display near-normal ultrastructural organization, with restored Z-line and sarcomere alignment. Scale bar (white) = 500nm.

Abbreviations: TEM, transmission electron microscopy; iPSC, induced pluripotent stem cell; CM, cardiomyocytes; Z, Z-disk.

3.6. Multi-electrode arrays and calcium transients in R205W corrected iPSC-CMs

FP traces data by MEA showed spontaneous beating trace for R205W and R205W^{Corr} iPSC-CMs line (**Figure 12A**). Compared to R205W iPSC-CMs, R205W^{Corr} iPSC-CMs exhibited a significantly increased mean of beat period (1.518 vs. 1.121 sec, p<0.001), indicating a decreased beating rate after gene correction. Spike amplitude was not statistically different between the two cell lines (4.374 vs. 4.149 mV, p=0.752). Conduction velocity was measured by MEA. The conduction plot revealed that R205W^{Corr} iPSC-CMs had faster conduction velocity than R205W iPSC-CMs (0.130 vs. 0.080 mm/ms, p<0.001) (**Figure 12B**), suggesting restoration of the propagation delay which indicates abnormal electrical signal transmission. Contractility was measured by MEA. The results indicated that R205W^{Corr} iPSC-CMs had increased beat amplitude (1.385 vs. 1.066%, p=0.001) and decreased E-C delay (257.6 vs. 293.5 ms, p=0.008) compared to R205W iPSC-CMs (**Figure 12C**). These findings suggest that the contractile force is restored and the time from electrical signal to contraction is reduced after gene correction. To measure the action potential of each contraction, the LEAP assay was measured by MEA. It was found that the R205W^{Corr} iPSC-CMs exhibited increased APD30, APD50, and APD90 values compared to R205W iPSC-CMs (**Figure 12D**).

For determining the spontaneous Ca^{2+} release features, the Ca^{2+} transient was further analyzed. Trace images displayed a change in Ca^{2+} transient for R205W and R205W^{Corr} iPSC-CMs (**Figure 13**). Quantitative analysis indicated that R205W^{Corr} iPSC-CMs had significantly higher systolic calcium (F/F_0) (7.123 vs. 2.685, p<0.001) and calcium amplitude (F/F_0) (6.312 vs. 1.715, p<0.001) than R205W iPSC-CMs (**Figure 13A**). Moreover, the time to baseline (50%) (0.587 vs. 0.501 sec, p=0.017) and relaxation constant Tau (sec) of calcium transient (0.441 vs. 0.365 sec, p=0.009) were significantly longer in R205W^{Corr} iPSC-CMs compared to R205W iPSC-CMs (**Figure 13B**),

indicating restoration of Ca^{2+} handling.

These experiments demonstrate that correcting TNNT2 R205W in DCM patient using iPSC-CM model with CRISPR-Cas9 gene editing affects not only structure but also electrophysiology and Ca^{2+} handling. Overall, these findings support the pathogenic effect of the TNNT2 R205W variant on the disease phenotype of DCM.

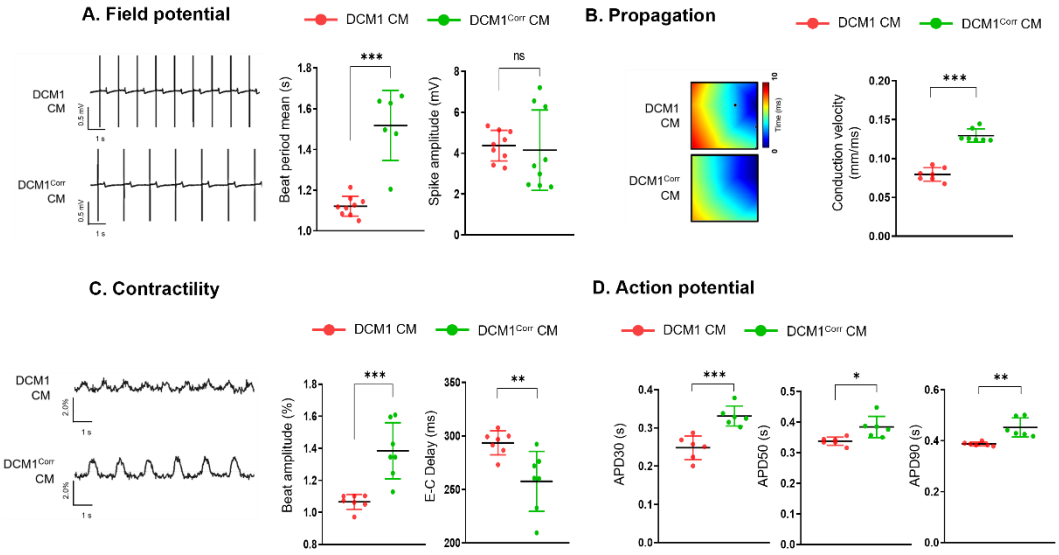

Figure 12. MEA was performed to confirm the electrophysiology in R205W and R205W^{Corr} iPSC-CMs. (A) Field potentials were measured by MEA. The mean of beat period was significantly increased in R205W^{Corr} iPSC-CMs (labeled as DCM1^{Corr}), while there was no difference in spike amplitude. (B) Conduction velocity was measured. R205W^{Corr} iPSC-CMs had significantly faster conduction velocity than R205W iPSC-CMs (labeled as DCM1). (C) Contractility was measured. Beat amplitude, which was significantly reduced in R205W iPSC-CMs, was significantly increased in R205W^{Corr} iPSC-CMs. E-C delay metric was also decreased in R205W^{Corr} iPSC-CMs compared to R205W iPSC-CMs. (D) The LEAP assay by MEA was performed to monitor action potential. Compared to R205W iPSC-CMs, APD30, APD50, and APD90 metrics were significantly increased in R205W^{Corr} iPSC-CMs. * $P < 0.05$, ** $P < 0.01$, *** $P < 0.001$ (Student's *t*-test).

Abbreviations: MEA, multi-electrode array; iPSC, induced pluripotent stem cell; CM, cardiomyocyte; E-C, excitation-contraction; LEAP, local extracellular action potential; ns, no significance.

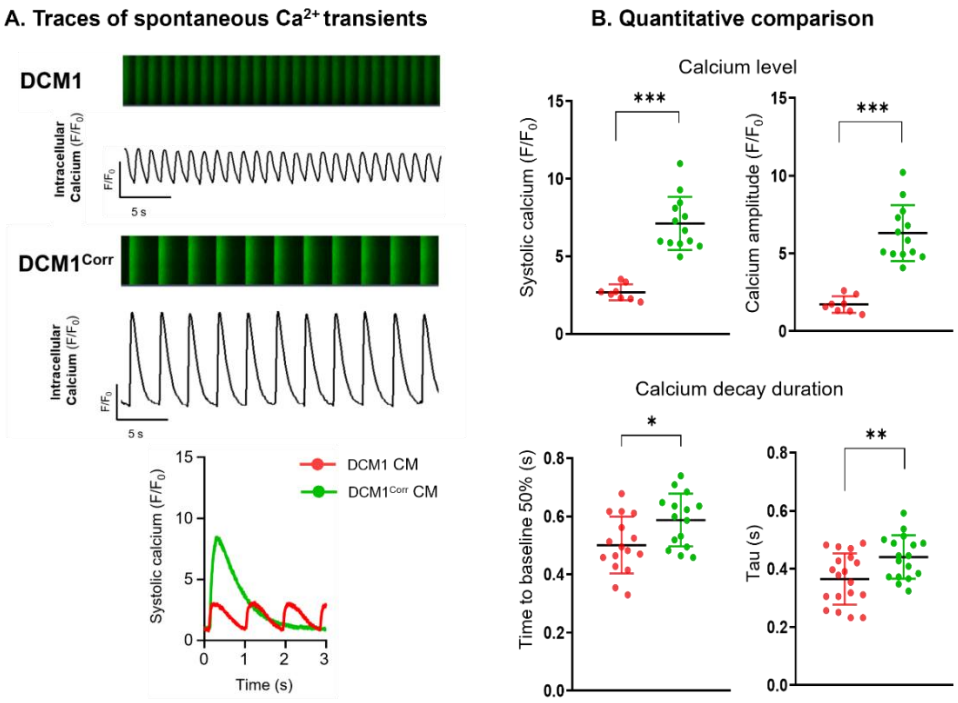

Figure 13. Calcium transient assay was performed in R205W and R205W^{Corr} iPSC-CMs.

Representative traces of spontaneous Ca^{2+} transients measured in R205W (labeled as DCM1) and R205W^{Corr} iPSC-CMs (labeled as DCM1^{Corr}). (A) The R205W^{Corr} iPSC-CMs had significantly increased systolic calcium and calcium amplitude compared to the R205W iPSC-CMs. (B) Also, time to baseline (50%) and relaxation constant Tau (sec) were significantly prolonged in R205W^{Corr} iPSC-CMs compared to R205W iPSC-CMs. * $P < 0.05$, ** $P < 0.01$, *** $P < 0.001$ (Student's *t*-test).

Abbreviations: iPSC, induced pluripotent stem cell; DCM, dilated cardiomyopathy; CM, cardiomyocytes.

4. Discussion

The findings of this study are as follows: First, iPSC-CMs derived from a patient carrying the TNNT2 R205W variant and a family history of cardiomyopathy exhibited an increased beating rate, reduced contractility, and impaired calcium transients compared to control iPSC-CMs. Additionally, CRISPR-Cas9-mediated correction of the R205W variant to the wild-type state resulted in the reversal of these phenotypes, aligning them with the control iPSC-CMs. Second, in the iPSC-CMs from a patient with the TNNT2 K210M variant, classified as VUS based on bioinformatics, no significant functional differences were observed in MEA compared to the control iPSC-CMs, contrasting the findings observed in the R205W model.

Genetic causes are crucial in DCM because the prognosis varies with different genetic variants. For example, variants in genes like LMNA or desmosomal genes increase the risk of sudden cardiac arrest and poor outcomes.[10] To date, there have been more than 100 identified definitive or strong causal genetic variants related to DCM.[48] With the advancements in NGS technology and the reduction in associated costs, the volume of genetic data is increasing rapidly.[4] Understanding the impact of each newly identified genetic variant on functional alterations and disease phenotypes remains a significant challenge. As the volume of genetic data continues to grow, the role of functional genomics—aimed at elucidating the correlation between genetic variants and phenotypes—becomes increasingly critical. Particularly, genetic variants in sarcomeric protein genes play a pivotal role in the pathogenesis of DCM (e.g. titin, myosin heavy chain, or troponin), highlighting the fundamental importance of the contractile machinery in cardiac function.[16][49][50]

As mentioned above, the TNNT2 gene encodes cTnT, a part the troponin complex which is commonly affected sarcomeric structures in DCM. Prior to the present study, several functional investigations have explored the relationship between TNNT2 variants and DCM. As mentioned

above, two studies focused on variants located at the same amino acid residue (position 205) as the R205W and reported altered Ca^{2+} sensitivity at the protein level using recombinant human protein or porcine cardiac-skinned fibers.[14)51)] Since the 2010s, the use of iPSC-CM models has enabled more detailed functional studies, which have demonstrated disease associated phenotypes, including sarcomere disarray, reduced contractility, and/or impaired Ca^{2+} handling in the context of TNNT2-related DCM.[31)52-54)] However, to date, no studies have performed gene correction of a causative TNNT2 variant to validate pathogenicity, and importantly, no functional studies have addressed VUS in this gene. In this study, I aimed to contribute to both mechanistic validation and clinical interpretation of TNNT2 variants in DCM. The interpretation of TNNT2 variants remains challenging due to the high proportion of rare missense variants and VUSs, which are often difficult to classify using standard *in silico* prediction tools.[38)] A recent study which used a transgenic sarcomere genomic platform to enable scalable interrogation of the TNNT2 variants showed that approximately 6.7% of the variants currently classified as pathogenic or likely pathogenic may be benign, while 9.5% of VUSs may have pathogenic potential. This finding is consistent with previous report suggesting that even likely pathogenic variants may carry false-positive rates of 10%,[55)] underscoring the need for re-evaluation not only of VUSs but also of variants already classified as likely pathogenic.

Importantly, when considering the TNNT2 R205W variant specifically, no prior studies have documented familial segregation of this variant in the context of DCM. To the best of current knowledge, the present study is the first to report a case in which both a father (Patient 1) and his daughter carried the identical R205W variant and exhibited concordant DCM phenotypes. This novel observation provides the first familial segregation evidence implicating the TNNT2 R205W variant in heritable forms of DCM and thus contributes an important layer of clinical validity to its pathogenic classification. However, genotyping was not performed for other family members, and

the limited sample size restricts definitive conclusions regarding penetrance. While full penetrance cannot be concluded, observed co-segregation in affected family members supports a causal relationship requiring larger pedigree-based evidence.

Additionally, how the observed genotype–phenotype correlations can be mechanistically explained remains uncertain and requires further investigation. In evaluating the pathogenicity of TNNT2 variants, several genetic aspects must be considered, including whether the disease follows a monogenic pattern and the inheritance mechanism. Although TNNT2-related cardiomyopathies are often viewed as monogenic disorders, the relationship is less consistent in DCM than HCM. Compared to HCM, which more commonly follows a clear monogenic inheritance pattern, DCM tends to exhibit greater heterogeneity and lower penetrance, making it inherently more challenging to attribute pathogenicity to individual variants.[56] Moreover, in the case of TNNT2-related DCM, the underlying pathogenic mechanism remains largely unexplored. While many reported TNNT2 variants are observed in the heterozygous state and appear to follow an autosomal dominant inheritance pattern, the actual disease-causing mechanism often remains speculative. Existing variant databases and published TNNT2 variant catalogs support the possibility that some heterozygous LoF variants act through haploinsufficiency, although dominant-negative mechanisms have also been proposed,[19)57)] particularly for missense mutations that impact sarcomeric integrity or calcium sensitivity. Although the TNNT2 gene shows a pLI score of 0, which statistically suggests tolerance to protein-truncating variants, this interpretation warrants caution. The apparent tolerance may reflect the low frequency of truncating variants in the population and a limited dataset rather than true biological tolerance. Importantly, pathogenic variants associated with TNNT2-related DCM are overwhelmingly missense rather than truncating,[18)] indicating that loss-of-function may not be the predominant disease mechanism. Therefore, focusing on the mechanistic implications of missense variants—as in the case of the patient studied here—is more relevant. The functional

experiments performed in this study were designed specifically to explore the pathogenic impact of such missense variants at the cellular and sarcomeric levels.

Therefore, to investigate clinical relevance of mutation-specific mechanisms, functional studies are essential to uncover the pathogenic potential of TNNT2 variants, because gene-level constraint scores (e.g. pLI score) appear discordant with phenotypic findings. In our study, the R205W iPSC-CMs exhibited shortened sarcomere length along with functional changes, both of which were restored upon gene correction to the wild-type sequence. Also, the ultrastructural disorganization observed in R205W iPSC-CMs provides direct morphological evidence that this variant disrupts sarcomeric architecture. Notably, restoration of near-normal ultrastructure following gene correction of the R205W variant strongly supports a causal relationship between this genetic alteration and the observed phenotype. These findings further substantiate the dominant-negative effect of the R205W variant, as the observed ultrastructural disorganization occurred in iPSC-CMs carrying the variant in a heterozygous state. This also support the hypothesis that its pathogenic mechanism may involve a mutation-specific effect, potentially mediated through disrupted protein–protein interactions within the sarcomere complex. Furthermore, Ca^{2+} transient assay revealed altered Ca^{2+} currents and MEA recordings showed a significant reduction in contractility, providing additional evidence that the structural disarray observed at the sarcomeric level translates into compromised cellular function. Therefore, these findings highlight the value of iPSC-based modeling combined with ultrastructural analysis in establishing functional relevance of candidate variants.

The present study has several limitations. One inherent limitation lies in the use of iPSC-CMs, which are known to be structurally and functionally immature compared to adult ventricular cardiomyocytes. Notably, iPSC-derived cardiomyocytes lack t-tubule structures and exhibit a reduced expression of key ion channels, resembling the electrophysiological profile of fetal-stage cardiomyocytes.[58-60] As a result, Ca^{2+} handling and contraction physiology in iPSC-CMs differ from

those observed in mature human cardiomyocytes, potentially affecting the interpretation of functional phenotypes. Moreover, patient-derived iPSC-CMs may exhibit reduced structural and functional maturation compared to those derived from healthy controls.[60] It is worth noting that patient-derived iPSC-CMs may exhibit greater immaturity or disrupted cellular physiology, which could be attributed not only to a specific gene variant but also to polygenic influences in differentiation conditions. Despite these potential confounding factors, the findings from our study remain meaningful. iPSC-CMs are generally characterized by a fetal-like electrophysiological profile, typically presenting with prolonged APD.[60] This electrophysiological immaturity is largely attributed to the reduced or absent inward rectifier potassium current, a well-known limitation of iPSC-derived cardiomyocytes.[60] In contrast, our disease model with the R205W variant demonstrated a marked shortening of APD, which deviates from this expected pattern and may indicate a variant-specific functional effect rather than a nonspecific feature of iPSC immaturity. Despite the inherent immaturity, the fact that most of the altered phenotypes observed in the present results were reversed in the gene-corrected iPSC-CMs strongly supports a high genotype–phenotype correlation. This key finding suggests that the observed functional changes are driven primarily by the genetic variant itself, rather than being a consequence of general immaturity in the iPSC-CM model. Another limitation of this study is the inability to accurately assess the penetrance of the TNNT2 variants due to incomplete genetic information from all family members. While the R205W variant was identified in two individuals with clear clinical phenotypes, suggesting possible segregation, definitive conclusions could not be drawn without genotypic data from the entire pedigree. Comprehensive genotype–phenotype correlation across affected and unaffected relatives would be necessary to more precisely evaluate variant penetrance and familial inheritance patterns. Further investigation will be necessary to elucidate the underlying pathophysiological mechanisms associated with these findings.

5. Conclusion

In this study, two TNNT2 heterozygous missense variants were functionally characterized using patient-derived iPSC-CMs, and both were evaluated to determine their potential to induce structural and functional abnormalities. The TNNT2 R205W variant was associated with disorganized sarcomeric architecture, shortened sarcomere length, altered Ca^{2+} currents, and reduced contractile function, all of which were substantially restored following CRISPR-Cas9-mediated correction. These findings provide strong support for a mutation-specific mechanism of pathogenicity and establish a direct causal link between the R205W variant and the DCM phenotype. In contrast, a nearby variant classified as a VUS, K210M, did not demonstrate clear structural or functional alterations, highlighting the power of this model to distinguish pathogenic variants from benign ones. These findings underscore the clinical utility of iPSC-CM-based functional assays in refining the classification of sarcomeric gene variants. Importantly, the value of iPSC-based disease modeling, particularly when combined with ultrastructural and functional analyses, is underscored in demonstrating the functional consequences of candidate variants in patients with suspected genetic cardiomyopathies.

References

1. Yan T, Zhu S, Yin X, et al. Burden, Trends, and Inequalities of Heart Failure Globally, 1990 to 2019: A Secondary Analysis Based on the Global Burden of Disease 2019 Study. *J Am Heart Assoc* 2023;12:e027852.
2. Virani SS, Alonso A, Aparicio HJ, et al. Heart Disease and Stroke Statistics-2021 Update: A Report From the American Heart Association. *Circulation* 2021;143:e254-e743.
3. Elliott P, Andersson B, Arbustini E, et al. Classification of the cardiomyopathies: a position statement from the European Society Of Cardiology Working Group on Myocardial and Pericardial Diseases. *Eur Heart J* 2008;29:270-6.
4. McNally EM, Mestroni L. Dilated Cardiomyopathy: Genetic Determinants and Mechanisms. *Circ Res* 2017;121:731-48.
5. Bozkurt B, Colvin M, Cook J, et al. Current Diagnostic and Treatment Strategies for Specific Dilated Cardiomyopathies: A Scientific Statement From the American Heart Association. *Circulation* 2016;134:e579-e646.
6. Ganesh SK, Arnett DK, Assimes TL, et al. Genetics and genomics for the prevention and treatment of cardiovascular disease: update: a scientific statement from the American Heart Association. *Circulation* 2013;128:2813-51.
7. Verdonschot JAJ, Hazebroek MR, Krapels IPC, et al. Implications of Genetic Testing in Dilated Cardiomyopathy. *Circ Genom Precis Med* 2020;13:476-87.
8. Hershberger RE, Hedges DJ, Morales A. Dilated cardiomyopathy: the complexity of a diverse genetic architecture. *Nat Rev Cardiol* 2013;10:531-47.
9. Burkett EL, Hershberger RE. Clinical and genetic issues in familial dilated cardiomyopathy. *J Am Coll Cardiol* 2005;45:969-81.
10. Gigli M, Merlo M, Graw SL, et al. Genetic Risk of Arrhythmic Phenotypes in Patients With

Dilated Cardiomyopathy. *J Am Coll Cardiol* 2019;74:1480-90.

11. Wakabayashi T. Mechanism of the calcium-regulation of muscle contraction--in pursuit of its structural basis. *Proc Jpn Acad Ser B Phys Biol Sci* 2015;91:321-50.
12. Mogensen J, Murphy RT, Shaw T, et al. Severe disease expression of cardiac troponin C and T mutations in patients with idiopathic dilated cardiomyopathy. *J Am Coll Cardiol* 2004;44:2033-40.
13. Pettinato AM, Ladha FA, Mellert DJ, et al. Development of a Cardiac Sarcomere Functional Genomics Platform to Enable Scalable Interrogation of Human TNNT2 Variants. *Circulation* 2020;142:2262-75.
14. Hershberger RE, Pinto JR, Parks SB, et al. Clinical and functional characterization of TNNT2 mutations identified in patients with dilated cardiomyopathy. *Circ Cardiovasc Genet* 2009;2:306-13.
15. Kamisago M, Sharma SD, DePalma SR, et al. Mutations in sarcomere protein genes as a cause of dilated cardiomyopathy. *N Engl J Med* 2000;343:1688-96.
16. Herman DS, Lam L, Taylor MR, et al. Truncations of titin causing dilated cardiomyopathy. *N Engl J Med* 2012;366:619-28.
17. Richards S, Aziz N, Bale S, et al. Standards and guidelines for the interpretation of sequence variants: a joint consensus recommendation of the American College of Medical Genetics and Genomics and the Association for Molecular Pathology. *Genet Med* 2015;17:405-24.
18. Mazzarotto F, Tayal U, Buchan RJ, et al. Reevaluating the Genetic Contribution of Monogenic Dilated Cardiomyopathy. *Circulation* 2020;141:387-98.
19. Watkins H, Seidman CE, Seidman JG, Feng HS, Sweeney HL. Expression and functional assessment of a truncated cardiac troponin T that causes hypertrophic cardiomyopathy.

Evidence for a dominant negative action. *J Clin Invest* 1996;98:2456-61.

20. Yang X, Pabon L, Murry CE. Engineering adolescence: maturation of human pluripotent stem cell-derived cardiomyocytes. *Circ Res* 2014;114:511-23.

21. Uosaki H, Taguchi YH. Comparative Gene Expression Analysis of Mouse and Human Cardiac Maturation. *Genomics Proteomics Bioinformatics* 2016;14:207-15.

22. Callaghan NI, Lee SH, Hadipour-Lakmehsari S, et al. Functional culture and in vitro genetic and small-molecule manipulation of adult mouse cardiomyocytes. *Commun Biol* 2020;3:229.

23. Zhou B, Shi X, Tang X, et al. Functional isolation, culture and cryopreservation of adult human primary cardiomyocytes. *Signal Transduct Target Ther* 2022;7:254.

24. Nikouee A, Yap JQ, Rademacher DJ, Kim M, Zang QS. An optimized Langendorff-free method for isolation and characterization of primary adult cardiomyocytes. *BMC Cardiovasc Disord* 2024;24:649.

25. Peters NS, Severs NJ, Rothery SM, Lincoln C, Yacoub MH, Green CR. Spatiotemporal relation between gap junctions and fascia adherens junctions during postnatal development of human ventricular myocardium. *Circulation* 1994;90:713-25.

26. Nishiga M, Qi LS, Wu JC. Therapeutic genome editing in cardiovascular diseases. *Adv Drug Deliv Rev* 2021;168:147-57.

27. Karakikes I, Ameen M, Termglinchan V, Wu JC. Human induced pluripotent stem cell-derived cardiomyocytes: insights into molecular, cellular, and functional phenotypes. *Circ Res* 2015;117:80-8.

28. Liu N, Olson EN. CRISPR Modeling and Correction of Cardiovascular Disease. *Circ Res* 2022;130:1827-50.

29. Fujino N, Shimizu M, Ino H, et al. Cardiac troponin T Arg92Trp mutation and progression

from hypertrophic to dilated cardiomyopathy. *Clin Cardiol* 2001;24:397-402.

30. Long PA, Evans JM, Olson TM. Diagnostic Yield of Whole Exome Sequencing in Pediatric Dilated Cardiomyopathy. *J Cardiovasc Dev Dis* 2017;4:11.

31. Clippinger SR, Cloonan PE, Greenberg L, Ernst M, Stump WT, Greenberg MJ. Disrupted mechanobiology links the molecular and cellular phenotypes in familial dilated cardiomyopathy. *Proc Natl Acad Sci U S A* 2019;116:17831-40.

32. Hanson EL, Jakobs PM, Keegan H, et al. Cardiac troponin T lysine 210 deletion in a family with dilated cardiomyopathy. *J Card Fail* 2002;8:28-32.

33. Landrum MJ, Lee JM, Benson M, et al. ClinVar: improving access to variant interpretations and supporting evidence. *Nucleic Acids Res* 2018;46:D1062-d7.

34. Gudmundsson S, Singer-Berk M, Watts NA, et al. Variant interpretation using population databases: Lessons from gnomAD. *Hum Mutat* 2022;43:1012-30.

35. Lek M, Karczewski KJ, Minikel EV, et al. Analysis of protein-coding genetic variation in 60,706 humans. *Nature* 2016;536:285-91.

36. Pollard KS, Hubisz MJ, Rosenbloom KR, Siepel A. Detection of nonneutral substitution rates on mammalian phylogenies. *Genome Res* 2010;20:110-21.

37. Siepel A, Bejerano G, Pedersen JS, et al. Evolutionarily conserved elements in vertebrate, insect, worm, and yeast genomes. *Genome Res* 2005;15:1034-50.

38. Adzhubei IA, Schmidt S, Peshkin L, et al. A method and server for predicting damaging missense mutations. *Nat Methods* 2010;7:248-9.

39. Ng PC, Henikoff S. Accounting for human polymorphisms predicted to affect protein function. *Genome Res* 2002;12:436-46.

40. Breckwoldt K, Letuffe-Brenière D, Mannhardt I, et al. Differentiation of cardiomyocytes and generation of human engineered heart tissue. *Nat Protoc* 2017;12:1177-97.

41. Sharma A, Li G, Rajarajan K, Hamaguchi R, Burridge PW, Wu SM. Derivation of highly purified cardiomyocytes from human induced pluripotent stem cells using small molecule-modulated differentiation and subsequent glucose starvation. *J Vis Exp* 2015;97:52628.

42. Hershberger RE, Parks SB, Kushner JD, et al. Coding sequence mutations identified in MYH7, TNNT2, SCN5A, CSRP3, LBD3, and TCAP from 313 patients with familial or idiopathic dilated cardiomyopathy. *Clin Transl Sci* 2008;1:21-6.

43. Rampersaud E, Siegfried JD, Norton N, Li D, Martin E, Hershberger RE. Rare variant mutations identified in pediatric patients with dilated cardiomyopathy. *Prog Pediatr Cardiol* 2011;31:39-47.

44. Jeon SB, Kim H, Chun KH, et al. Human induced pluripotent stem cell line YCMi007-A generated from a dilated cardiomyopathy patient with a heterozygous dominant c.613C > T (p. Arg205Trp) variant of the TNNT2 gene. *Stem Cell Res* 2023;67:103048.

45. Kim JH, Jo HY, Ha HY, Kim YO. Korea National Stem Cell Bank. *Stem Cell Res* 2021;53:102270.

46. Dabiri GA, Turnacioglu KK, Sanger JM, Sanger JW. Myofibrillogenesis visualized in living embryonic cardiomyocytes. *Proc Natl Acad Sci U S A* 1997;94:9493-8.

47. Hayes HB, Nicolini AM, Arrowood CA, et al. Novel method for action potential measurements from intact cardiac monolayers with multiwell microelectrode array technology. *Sci Rep* 2019;9:11893.

48. Gigli M, Stolfo D, Merlo M, Sinagra G, Taylor MRG, Mestroni L. Pathophysiology of dilated cardiomyopathy: from mechanisms to precision medicine. *Nat Rev Cardiol* 2025;22:183-98.

49. Anderson BR, Granzier HL. Titin-based tension in the cardiac sarcomere: molecular origin and physiological adaptations. *Prog Biophys Mol Biol* 2012;110:204-17.

50. Pugh TJ, Kelly MA, Gowrisankar S, et al. The landscape of genetic variation in dilated cardiomyopathy as surveyed by clinical DNA sequencing. *Genet Med* 2014;16:601-8.

51. Pan S, Sommese RF, Sallam KI, et al. Establishing disease causality for a novel gene variant in familial dilated cardiomyopathy using a functional in-vitro assay of regulated thin filaments and human cardiac myosin. *BMC Med Genet* 2015;16:97.

52. Sun N, Yazawa M, Liu J, et al. Patient-specific induced pluripotent stem cells as a model for familial dilated cardiomyopathy. *Sci Transl Med* 2012;4:130ra47.

53. Dai Y, Amenov A, Ignatyeva N, et al. Troponin destabilization impairs sarcomere-cytoskeleton interactions in iPSC-derived cardiomyocytes from dilated cardiomyopathy patients. *Sci Rep* 2020;10:209.

54. Jung P, Seibertz F, Fakuade FE, et al. Increased cytosolic calcium buffering contributes to a cellular arrhythmogenic substrate in iPSC-cardiomyocytes from patients with dilated cardiomyopathy. *Basic Res Cardiol* 2022;117:5.

55. Harrison SM, Rehm HL. Is 'likely pathogenic' really 90% likely? Reclassification data in ClinVar. *Genome Med* 2019;11:72.

56. Burke MA, Cook SA, Seidman JG, Seidman CE. Clinical and Mechanistic Insights Into the Genetics of Cardiomyopathy. *J Am Coll Cardiol* 2016;68:2871-86.

57. Oberst L, Zhao G, Park JT, et al. Dominant-negative effect of a mutant cardiac troponin T on cardiac structure and function in transgenic mice. *J Clin Invest* 1998;102:1498-505.

58. Kane C, Couch L, Terracciano CM. Excitation-contraction coupling of human induced pluripotent stem cell-derived cardiomyocytes. *Front Cell Dev Biol* 2015;3:59.

59. Gherghiceanu M, Barad L, Novak A, et al. Cardiomyocytes derived from human embryonic and induced pluripotent stem cells: comparative ultrastructure. *J Cell Mol Med* 2011;15:2539-51.

60. Schick R, Mekies LN, Shemer Y, et al. Functional abnormalities in induced Pluripotent Stem Cell-derived cardiomyocytes generated from titin-mutated patients with dilated cardiomyopathy. *PLoS One* 2018;13:e0205719.

Abstract in Korean

확장성 심근병증 환자 유래 유도만능줄기세포 기반 심근세포 모델을 활용한 TNNT2 유전자 변이의 기능적 검증 연구

본 연구는 확장성 심근병증(Dilated Cardiomyopathy, DCM)과 관련된 TNNT2 유전자 변이의 병원성 평가를 위해 환자 유래 전분화능 줄기세포(induced pluripotent stem cell; iPSC) 기반 심근세포(cardiomyocytes; CMs) 모델을 구축하고, 기능적 분석을 수행한 연구이다. DCM은 심실 확장과 수축기 기능 저하를 특징으로 하며, 약 30-50%가 유전적 요인과 연관되어 있다. 특히 TNNT2 유전자는 트로포닌 복합체 구성 요소로, 근절(sarcomere) 단백질 중 DCM과 연관된 대표 유전자 중 하나이나, 그 변이에 대한 기능적 데이터는 제한적이며, 그 중 많은 변이들이 임상적 의의가 불확실한 변이(Variants of Uncertain Significance; VUSs)로 분류되어 있다. 본 연구에서는 TNNT2 변이를 가진 환자 2명을 대상으로 각 변이(p.Arg205Trp; R205W, p.Lys210Met; K210M)에 대해 iPSC를 제작하고, 이를 심근세포로 분화시켜 기능 분석을 수행하고자 하였다.

연구 대상 환자는 DCM 코호트 내에서 시행한 유전체 분석 선별을 통해 선정하였다. TNNT2 변이를 지닌 환자들 중, 병원성이 확실시되거나, VUS 중에서도 병원성이 의심되지 않는 변이들은 제외하였고, 각각 likely pathogenic 및 VUS 로 분류된 TNNT2 변이(각각 R205W, K210M)를 연구 대상 변이로 선정하였다. 기능적 변화를 검증하기 위해, 2017년에 한국줄기세포은행에 보관된 CMC-iPSC-

011 계열의 건강한 공여자로부터 유래한 iPSCs(이하, 대조 세포주)를 사용하였다. R205W, K210M 변이를 지닌 환자 혈액으로부터 제작된 iPSC와 대조 세포주로부터 표준화된 심근세포 분화 프로토콜을 통해 iPSC-CM가 유도되었고, pluripotency marker 및 sarcomere 단백질(cTnT, titin, α-actinin) 발현을 확인하였다. 변이의 기능적 분석을 위해 전기생리학적 측정(multi-electrode array; MEA), 칼슘 흐름 분석, sarcomere 길이 측정 등을 수행하였다. 또한 R205W 변이에 대해서는 CRISPR-Cas9 기반 유전자 교정을 수행하여 wild-type으로 복구된 isogenic 세포주($R205W^{Corr}$)를 구축하였으며, 동일한 분석 방법으로 기능적 비교를 수행하고자 하였다.

R205W 변이를 가진 iPSC-CMs는 대조 세포주 심근세포와 비교하여 빠른 박동률, 낮은 수축력, 느린 전도 속도, 그리고 칼슘 유입 및 배출의 이상을 보였으며, action potential duration(APD) 또한 비정상적으로 짧아지는 현상이 관찰되었다. 이는 iPSC immaturity에서 흔히 보이는 패턴과는 다른 결과로, 해당 변이가 전기생리학적 기능 이상을 유발함을 시사한다. 반면, K210M 변이를 가진 iPSC-CMs는 박동 주기에서만 경미한 차이를 보였고, 전도 속도나 수축력에서는 유의한 차이를 보이지 않아 기능적으로 병리성을 뒷받침하기 어려운 결과를 나타냈다. 추가적인 세포내 칼슘 흐름 분석에서, R205W 변이를 가진 iPSC 유래 심근세포에서는 대조 세포주 심근세포 대비 칼슘 신호 주기가 정상 세포에 비해 현저히 짧았으며, 수축기 칼슘 신호의 진폭 또한 유의하게 감소한 양상을 보였다. 이러한 변화는 심근세포 내 칼슘 조절 기능의 장애를 반영하며, 수축기 기능 저하와 밀접한 관련이 있는 것으로 생각되었다. R205W 변이에 대해 CRISPR-Cas9 방법을

통해 wild-type으로 교정하였을 때 해당 변화가 어떻게 다시 달라지는지 확인하고자 하였고, 유전자 교정을 통해 복구된 R205W^{Corr} iPSC-CMs에서는 이러한 기능적 변화가 대부분 정상화되어, R205W 변이의 병인성을 지지하는 강력한 근거를 제시하였다.

이러한 결과는 DCM 환자를 대상으로 한 TNNT2 유전자 변이의 기능적 영향에 대한 정량적 비교 및 교정 후 회복 효과를 최초로 보고한 사례로, 특히 VUS 변이의 기능적 평가에 대한 새로운 가능성을 제시하였다. 이를 통해 R205W 변이는 sarcomere 구조 및 칼슘 조절에 영향을 주며, 이는 DCM에서 중심적인 병태생리인 수축기능 저하와 밀접히 연결된다는 것을 알 수 있었다. iPSC-CM 기반의 기능 분석 플랫폼은 향후 변이의 병원성 재분류 및 정밀 유전 진단에 있어 중요한 역할을 할 수 있으며, 유전자 기반 맞춤 치료 전략 수립을 위한 기반 연구로서 의의가 크다고 할 수 있겠다.

핵심되는 말: 심근병증, 유전자, 변이, 유도만능줄기세포, 심근세포, TNNT2, CRISPR-Cas9